Chinmo defines the region-specific oncogenic competence in the *Drosophila* central nervous system

Phuong-Khanh Nguyen[1,2], Francesca Froldi[1,2], Louise Y Cheng[1,2,3,#]

1. Sir Peter MacCallum Department of Oncology, The University of Melbourne, VIC 3010, Australia
2. Peter MacCallum Cancer Centre, Melbourne, VIC 3000, Australia
3. Department of Anatomy and Physiology, The University of Melbourne, VIC 3010, Australia

Corresponding author

Email: louise.cheng@petermac.org

Keywords: *Drosophila*, dedifferentiation, terminal differentiation, malignancy

Running title: Oncogenic competence of dedifferentiated neuroblasts

Abstract

While genetic mutations can promote hyperplastic growth, they do not always result in oncogenesis characterized by uncontrolled cell proliferation. Dedifferentiation, the process by which mature cells revert to a multipotent state, holds great potential for regeneration but also poses a risk of tumorigenesis. The factors that determine these opposing outcomes, however, remain unknown. We and others have previously identified the transcription factors Nerfin-1 and Lola as inhibitors of dedifferentiation. Here, we investigate how the oncogenic potential of dedifferentiation varies across different neural lineages in the *Drosophila* central nervous system (CNS). We found that Nerfin-1 inactivation causes oncogenic phenotypes in the central brain (CB) and the ventral nerve cord (VNC) but not optic lobe (OL). In contrast, Lola inactivation leads to tumour overgrowth specifically in the OL. We identify Chinmo, an oncogenic temporal transcription factor, and its regulation by ecdysone signalling as key determinants of these differential responses. Together, our findings reveal a mechanism by which the regulation of temporal factors like Chinmo influences the tumorigenic outcome of dedifferentiation. This provides a fundamental framework to understand how oncogenic competence arises beyond genetic mutations.

Introduction

Genetic mutations are not the sole determinants of malignant cancer outcomes. In fact, individuals can accumulate mutations with oncogenic potential, yet most are eliminated without leading to malignancy. Oncogenic competence is defined by a combination of genetic mutations, lineage-specific factors, and microenvironmental cues (Pavinato & Baggiolini, 2025). Many brain and central nervous system (CNS) cancers originate from excessively proliferative neural stem-progenitor cells during embryonic development (Bruschi et al., 2021; Marshall et al., 2014). Perturbations in signalling pathways and transcription factors involved in neural development can initiate tumour overgrowth in the CNS (Chen et al., 2024). Interestingly, distinct oncogenic mutations are associated with specific anatomical regions of the CNS (Gibson et al., 2010; Mackay et al., 2017; Sturm et al., 2012), suggesting that oncogenic competence is regionally regulated. However, the mechanisms by which region-specific cues influence cancerous transformation remain poorly understood.

The *Drosophila* CNS is a well-established model for studying neurogenesis, cell fate specification, and maintenance during development. In *Drosophila*, neural stem cell-like progenitors, known as neuroblasts (NBs), generate neurons and glia across all regions of the CNS. Here, the CNS is broadly divided into three main regions: the ventral nerve cord (VNC), the central brain (CB), and the optic lobes (OLs) (Figure 1A). From embryonic to mid-pupal development, NBs undergo a limited number of divisions until their termination, by which the mechanism differs between regions (Hofbauer & Campos-Ortega, 1990; Ito & Hotta, 1992; Truman & Bate, 1988). In the CB/VNC, NB termination mainly occurs via terminal symmetric division mediated by the homeobox transcription factor Prospero (Pros) (Maurange et al., 2008). Whereas in the optic lobe (OL), medulla NBs undergo termination through a combination of apoptosis, terminal symmetric division, and gliogenic switch (Nguyen & Cheng, 2024). Thus, NBs terminate in a region-specific fashion to meet the differential demands of neuronal function during adulthood.

Multiple studies have shown that temporal transcription factors (tTFs) and their target genes regulate NB termination in the CB and the VNC. These tTFs are sequentially expressed in NBs as they age, not only specifying distinct neuronal identities in their progeny but also influencing cell cycle speed and the timing of NB termination. For instance, during early larval development, NBs in the CB/VNC express early temporal factors: IGF-II mRNA-binding proteins (Imp) and the BTB-zinc finger transcription factor Chronologically inappropriate morphogenesis (Chinmo) (Maurange et al., 2008; Ren et al., 2017; Syed et al., 2017). As the animal matures, NBs shift to express late temporal factors, namely Syncrip (Syp) and Broad (Br) (Maurange et al., 2008; Ren et al., 2017; Syed et al., 2017). Imp and Syp modulate NB proliferation through opposing gradients, with Imp promoting the proliferation whereas Syp driving the termination of NBs (Syed et al., 2017; Yang et al., 2017). Thus, an extended period of Imp expression or inhibition of Syp can prolong NB proliferation (Yang et al., 2017).

Temporal patterning is also observed in the OL medulla in which Imp and Chinmo define the early temporal window, while Syp, Br, and Eip93F define the late temporal window (Arain et al., 2022; Dillard et al., 2018; Zhou et al., 2019). However, it is unclear if this temporal cascade influences medulla NB termination.

In this study, we investigate how dedifferentiation - triggered by the loss of neuronal cell fate maintenance – can lead to contrasting tumorigenic outcomes. Previously, we and others have shown that neuronal cell fate requires active maintenance by various transcription factors, such as the zinc finger transcription factor Nervous finger 1 (Nerfin-1) and the BTB-zinc finger transcription factor Longitudinals lacking (Lola) (Froldi et al., 2015; Vissers et al., 2018; Xu et al., 2017; Southall et al., 2014). Failure to maintain the neuronal identity can result in the formation of supernumerary NBs that can drive tumour overgrowth. Here, we demonstrate that oncogenic competence of dedifferentiated NBs is region-specific. In the CB and VNC, the loss of Nerfin-1 function leads to malignant tumour overgrowth, with ectopic NBs continuing to proliferate beyond the normal neurogenesis period (Froldi et al., 2015). In contrast, in the OLs, we show that ectopic NBs are eliminated through apoptosis-mediated cell death and differentiation. Unlike Nerfin-1, Lola loss-of-function elicits tumorigenesis in the adult OL (Southall et al., 2014). Mechanistically, we identified the early tTF Chinmo and ecdysone signalling as key determinants of this differential response. Increasing Chinmo levels confers oncogenic competence to dedifferentiated NBs induced by Nerfin-1 inactivation in the OL. Conversely, reducing Chinmo levels in those in the CB/VNC or in *lola*$^{-/-}$ clones promote elimination of dedifferentiated NBs. These findings highlight that the differential expression and regulation of oncogenic tTFs such as Chinmo, play a crucial role in determining tumorigenic outcome in response to dedifferentiation triggers. Overall, our study shed light on mechanisms of oncogenic competency and offers insights into how certain regions of the brain are more susceptible to tumorigenesis than others.

Results

nerfin-1 loss-of-function (*nerfin-1*^{159}) causes malignant tumour overgrowth in the CB/VNC but not the OL

We and others have previously reported that *nerfin-1* loss-of-function leads to the dedifferentiation of neurons into ectopic NBs (Froldi et al., 2015; Vissers et al., 2018; Xu et al., 2017). In this study, to investigate region-specific regulation of dedifferentiation, we began by inducing *nerfin-1*^{159}-null mutant loss-of-function clones at 24 hrs ALH (After Larval Hatching) via heat-shock MARCM in all the regions of the larval CNS (CB, VNC, and OLs) (Figure 1A-B). At wandering L3 stage, ectopic Deadpan (Dpn^{+}) NBs were found in the deep sections of *nerfin-1*^{159} clones in all the regions of the brain (Figure 1A', C-D), indicative of neuronal reversion into NBs. In the developing CB/VNC, NBs terminally differentiate at around 24 hrs after pupal formation (APF) (Maurange et al., 2008) whereas medulla

Figure 1

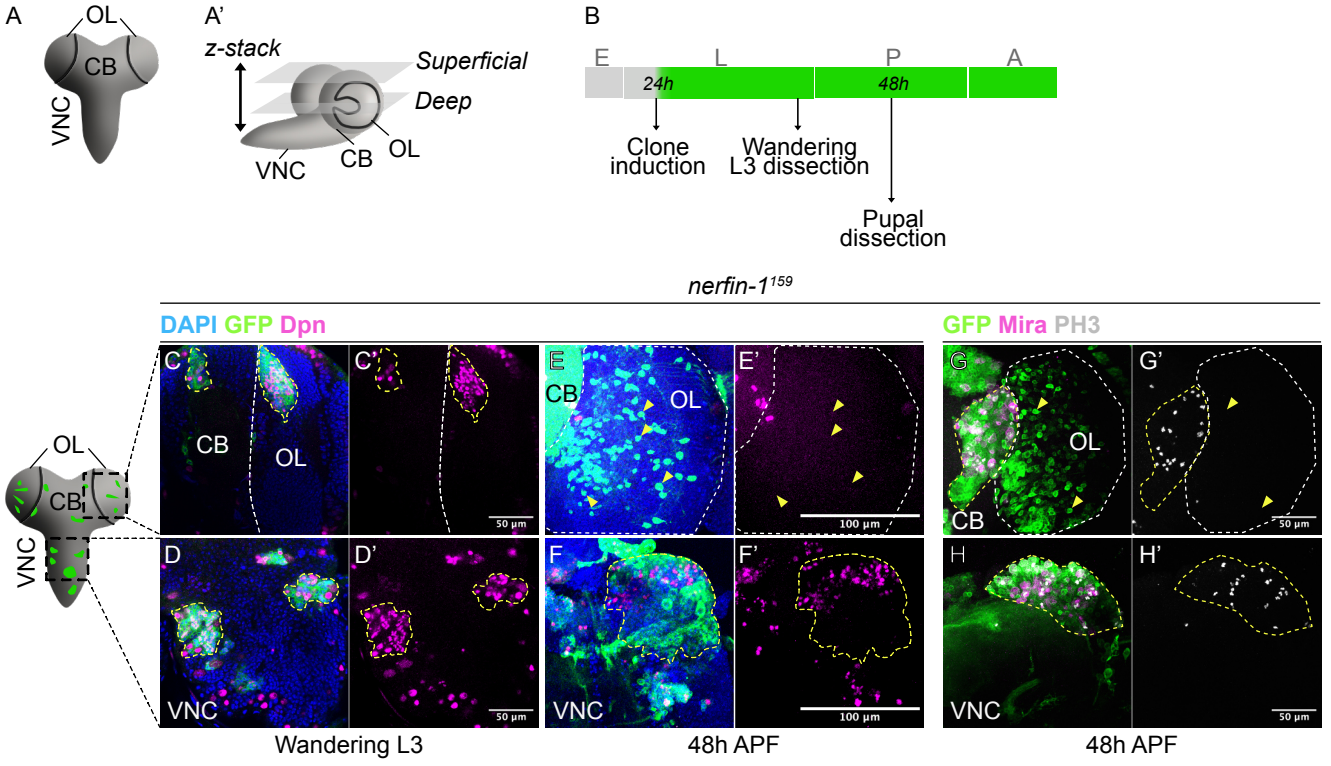
A
OL
CB
VNC
A'
z-stack
Superficial
Deep
VNC
CB
OL
B
E
L
P
A
24h
48h
Clone induction
Wandering L3 dissection
Pupal dissection
nerfin-1159
DAPI GFP Dpn
GFP Mira PH3
C
C'
CB
OL
50 µm
E
E'
CB
OL
100 µm
G
G'
OL
CB
50 µm
D
D'
VNC
50 µm
F
F'
VNC
100 µm
H
H'
VNC
50 µm
Wandering L3
48h APF
48h APF

NBs of the OL terminate between 12-24 hrs APF (Nguyen & Cheng, 2024). A key characteristic of malignant tumours is their failure to obey signals to terminally differentiate and their ability to proliferate beyond the normal period of neurogenesis. To examine these characteristics, we analysed the brains at 48 hrs APF and found that *nerfin-1*^{159} clones in the CB and the VNC were enriched with ectopic Dpn^{+} NBs (Figure 1B, E-F). Conversely, in the OL, *nerfin-1*^{159} clones were devoid of Dpn and became dispersed across the OL, indicative of neuronal differentiation and migration akin to the wildtype context (Morante et al., 2011) (Figure 1E-E', yellow arrowheads). To ascertain whether *nerfin-1*^{159} NBs undergo proliferation beyond the normal period of neurogenesis, we stained the pupal brains at 48 hrs APF for proliferative NBs marked by Miranda (Mira) and Phospho-Histone 3 (PH3). We found that Mira^{+} PH3^{+} NBs were present in *nerfin-1*^{159} clones in the CB and the VNC (Figure 1G-H) but absent in those in the OL (Figure 1G-G', yellow arrowheads), suggesting that proliferation is sustained only in the pupal CB/VNC. Together, our data reveal that the same genetic mutation (*nerfin-1*^{159}) can cause differential consequences in a region-specific manner: dedifferentiated NBs drive tumorigenic overgrowth in the CB/VNC but are eliminated in the OL.

nerfin-1^{159} dedifferentiated NBs in the OL are eliminated via a combination of Pros-mediated differentiation and apoptosis-mediated cell death

To test how *nerfin-1*^{159} dedifferentiated NBs become eliminated in the pupal OL, we examined whether these NBs undergo differentiation or a gliogenic switch – mechanisms responsible for wildtype medulla NB termination (Nguyen & Cheng, 2024). First, we assayed for the expression of the neuronal marker Elav and glial marker Repo in *nerfin-1*^{159} clones at 48 hrs APF. We found that *nerfin-1*^{159} clones contained Elav^{+} neurons (Figure 2A-B, cyan arrowheads) and Repo^{+} glial cells (Figure 2A-B, magenta arrowheads) in both pupal OL and VNC. However, the rate of neuronal differentiation (percentage of Elav^{+} neurons per region) was significantly higher in the OL than the VNC at 48 hrs APF (Figure 2C). To address whether terminal differentiation is necessary for the elimination of *nerfin-1*^{159} dedifferentiated NBs in the pupal OL, we knocked down the transcription factor Pros, which has been shown to mediate NB terminal differentiation via symmetric division (Maurange et al., 2008; Nguyen & Cheng, 2024). At wandering L3 stage, in the deep layers of the OLs, ectopic NBs were found in *nerfin-1*^{159}, *pros*^{RNAi} and *pros*^{RNAi}*;nerfin-1*^{159} clones (Figure 1C, 2D-E). At 48 hrs APF, in contrast to *nerfin-1*^{159} clones, *pros*^{RNAi}*;nerfin-1*^{159} clones exhibited persistent ectopic NBs in the OL (Figure 2F, H, J), suggesting that Pros may be required for the elimination of *nerfin-1*^{159} dedifferentiation NBs. However, persistent ectopic NBs were also observed in *pros*^{RNAi} clones (Figure 2F, H, J), which reflects the fact that Pros acts upstream of Nerfin-1 in the differentiation cascade as we have previously shown (Froldi et al., 2015). To elucidate whether the gliogenic switch also plays a role in the elimination of *nerfin-1*^{159} dedifferentiated NBs, we knocked down the glial cell fate determinant Glial-cell-missing

Figure 2

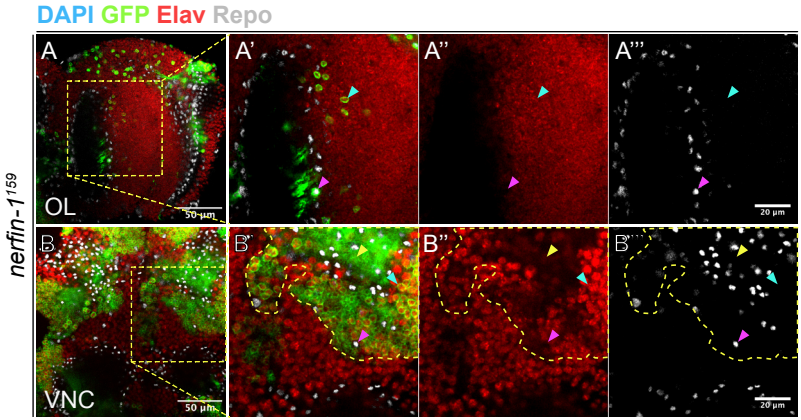

48h APF

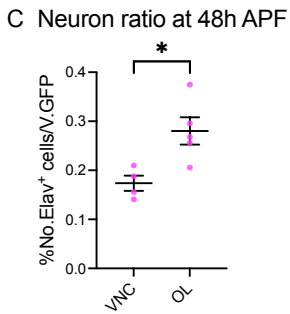

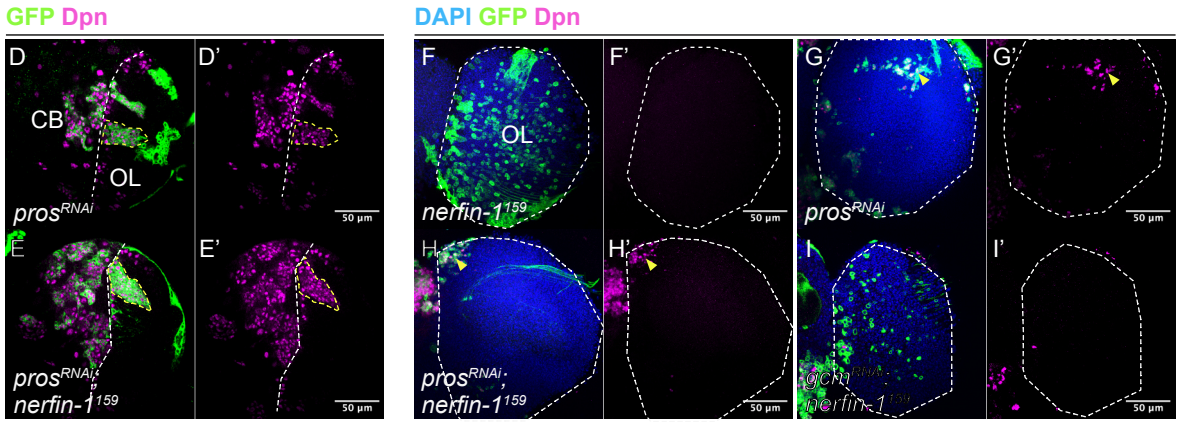

Wandering L3

48h APF

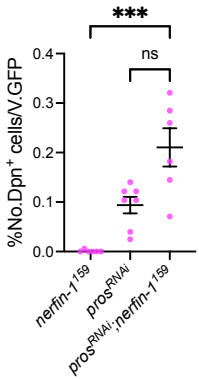

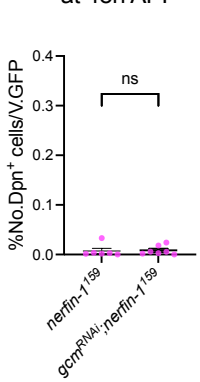

(Gcm) by RNAi. This manipulation did not significantly increase the persistence of ectopic NBs at 48 hrs APF (Figure 2F, I-K). Hence, an acquisition of the glial cell fate is not necessary to eliminate *nerfin-1*^{159} dedifferentiated NBs in the pupal OL.

A subset of NBs in the developing OL terminates via apoptosis-mediated cell death during early pupal development (Nguyen & Cheng, 2024). At wandering L3 stage, we found that some dedifferentiated NBs in *nerfin-1*^{159} clones expressed the apoptotic marker Caspase-1 (Dcp-1) (Supplementary Figure 1A-A', arrowheads). To address if apoptosis is required for the elimination of *nerfin-1*^{159} dedifferentiated NBs, we inhibited apoptosis by overexpressing the apoptotic inhibitor p35 in *nerfin-1*^{159} clones. This perturbation exhibited no Dcp-1 expression in the dedifferentiated NBs at wandering L3 stage, indicating that apoptosis was suppressed (Supplementary Figure 1B-B'). Additionally, there was a small increase in the NB ratio in *p35;nerfin-1*^{159} clones in the OLs compared to *nerfin-1*^{159} at 48 hrs APF (Supplementary Figure 1C-E). Notably, many *UAS-p35;nerfin-1*^{159} cells in the pupal OLs were devoid of Dpn expression (Supplementary Figure 1D-D', white arrowheads), suggesting that the cells that do not die may still undergo terminal differentiation. Together, our data suggest that the primary mechanism for the elimination of *nerfin-1*^{159} dedifferentiated NBs in the pupal OL involves a combination of Pros-mediated terminal differentiation and apoptosis.

The elimination *of nerfin-1*^{159} dedifferentiated NBs in the pupal OL occurs independently of Myc

In the VNC, we previously showed that *nerfin-1*^{159}-induced neuronal dedifferentiation is dependent on the expression of the growth regulator Myc (Froldi et al., 2015). Interestingly, our immunostaining showed that Myc was expressed in *nerfin-1*^{159} clones in the CB and VNC but not in the OL at wandering L3 stage (Supplementary Figure 1F-G). Hence, it is plausible the elimination of *nerfin-1*^{159} dedifferentiated NBs in the pupal OL is caused by the lack of Myc. To test this hypothesis, we overexpressed Myc in *nerfin-1*^{159} clones. While this manipulation was sufficient to increase Myc levels in *nerfin-1*^{159} clones in the OL (Supplementary Figure 1H-I, arrowheads), it was not sufficient to promote the persistence of ectopic NBs at 48 hrs APF (Supplementary Figure 1E, H, I). Therefore, the absence of Myc expression in *nerfin-1*^{159} clones in the OL does not contribute to the elimination of dedifferentiated NBs during pupal development.

The elimination *of nerfin-1*^{159} dedifferentiated NBs in the pupal OL is due to the absence of the oncogenic temporal factor Chinmo

In the VNC, the malignant tumour competency is determined by the expression of the oncogenic tTF Chinmo, such that cells generated during the Imp^{+}Chinmo^{+} window are susceptible to malignant tumour overgrowth (Genovese et al., 2019; Narbonne-Reveau et al., 2016). Whereas late-born cells from the

169 $Syp^{+}Br^{+}$ temporal window have the propensity to undergo terminal differentiation. To investigate if
170 Chinmo is involved in the elimination of *nerfin-1*^{159} dedifferentiated NBs in the pupal OL, we first
171 examined Chinmo expression in *nerfin-1*^{159} clones at wandering L3 stage. Consistent with previous
172 reports (Narbonne-Reveau et al., 2016), we found that Chinmo was expressed in *nerfin-1*^{159}
173 dedifferentiated NBs in the CB and the VNC (Figure 3A-B). In contrast, *nerfin-1*^{159} dedifferentiated
174 NBs in the OL did not express Chinmo (Figure 3C-C").

175 To test whether Chinmo is functionally required to promote the persistence of dedifferentiated
176 NBs in the CB/VNC, we expressed *chinmo*^{RNAi} (see Materials and methods for details of RNAi
177 construction) in *nerfin-1*^{159} clones. At wandering L3 stage, the expression of *chinmo*^{RNAi} effectively
178 reduced Chinmo levels in *nerfin-1*^{159} clones in the VNC (Figure 3D-E). At 48 hrs APF,
179 *chinmo*^{RNAi}*;nerfin-1*^{159} clones displayed a significant reduction in the NB ratio in the CB/VNC
180 compared to *nerfin-1*^{159} clones (Figure 3F-H). Hence, Chinmo is required to promote tumorigenesis of
181 *nerfin-1*^{159} dedifferentiated NBs in the pupal CB/VNC. Next, we sought to address whether the absence
182 of Chinmo accounts for the elimination of *nerfin-1*^{159} dedifferentiated NBs in the pupal OL. To do so,
183 we overexpressed a full-length version of *chinmo* (*chinmo*^{FL}) (S. Zhu et al., 2006) in *nerfin-1*^{RNAi} flip-
184 out clones. By 24 hrs APF, *nerfin-1*^{RNAi}*;mCherry*^{RNAi} control clones in the OL were devoid of Dpn
185 expression and cells were dispersed across the OLs (Figure 3I). Conversely, *nerfin-1*^{RNAi};*chinmo*^{FL}
186 clones contained persistent ectopic NBs, resulting in significantly increased NB ratio compared to the
187 *nerfin-1*^{RNAi}*;mCherry*^{RNAi} counterparts (Figure 3I-K). Therefore, Chinmo is sufficient to prevent the
188 elimination of *nerfin-1* loss-of-function NBs in the pupal OL. Collectively, our data highlight the role
189 of Chinmo in conferring oncogenic competence in dedifferentiated NBs.

190

191 **Chinmo is repressed by ecdysone signalling in *nerfin-1*^{159} clones in the OL**

192 We next investigated how Chinmo expression is regulated in *nerfin-1*^{159} clones in the OL. In the
193 developing OL medulla, Chinmo has been shown to be expressed from early to mid-larval stages (Arain
194 et al., 2022; Dillard et al., 2018), the time window in which mutant clones are usually induced. As
195 *nerfin-1*^{159} clones in the larval OL were devoid of Chinmo expression (Figure 3C), a mechanism must
196 be present to repress Chinmo. To elucidate this, we first examined whether *chinmo* expression is
197 regulated by transcriptional or post-transcriptional mechanisms. We utilised a reporter in which the
198 mCherry coding sequence is flanked by the 5' and 3' UTRs of *chinmo* (*UAS-mCherry-chinmo*^{UTRs})
199 (Dillard et al., 2018). If *chinmo* is regulated post-transcriptionally, it is expected that clones would not
200 express mCherry. At wandering L3 stage, we found that both wildtype and *nerfin-1*^{RNAi} flip-out clones
201 expressed mCherry (Supplementary Figure 2A-B). These results suggest that Chinmo expression is
202 regulated via transcriptional rather than post-transcriptional mechanisms in both wildtype and *nerfin-*
203 *1*^{159} cells in the OL.

Figure 3

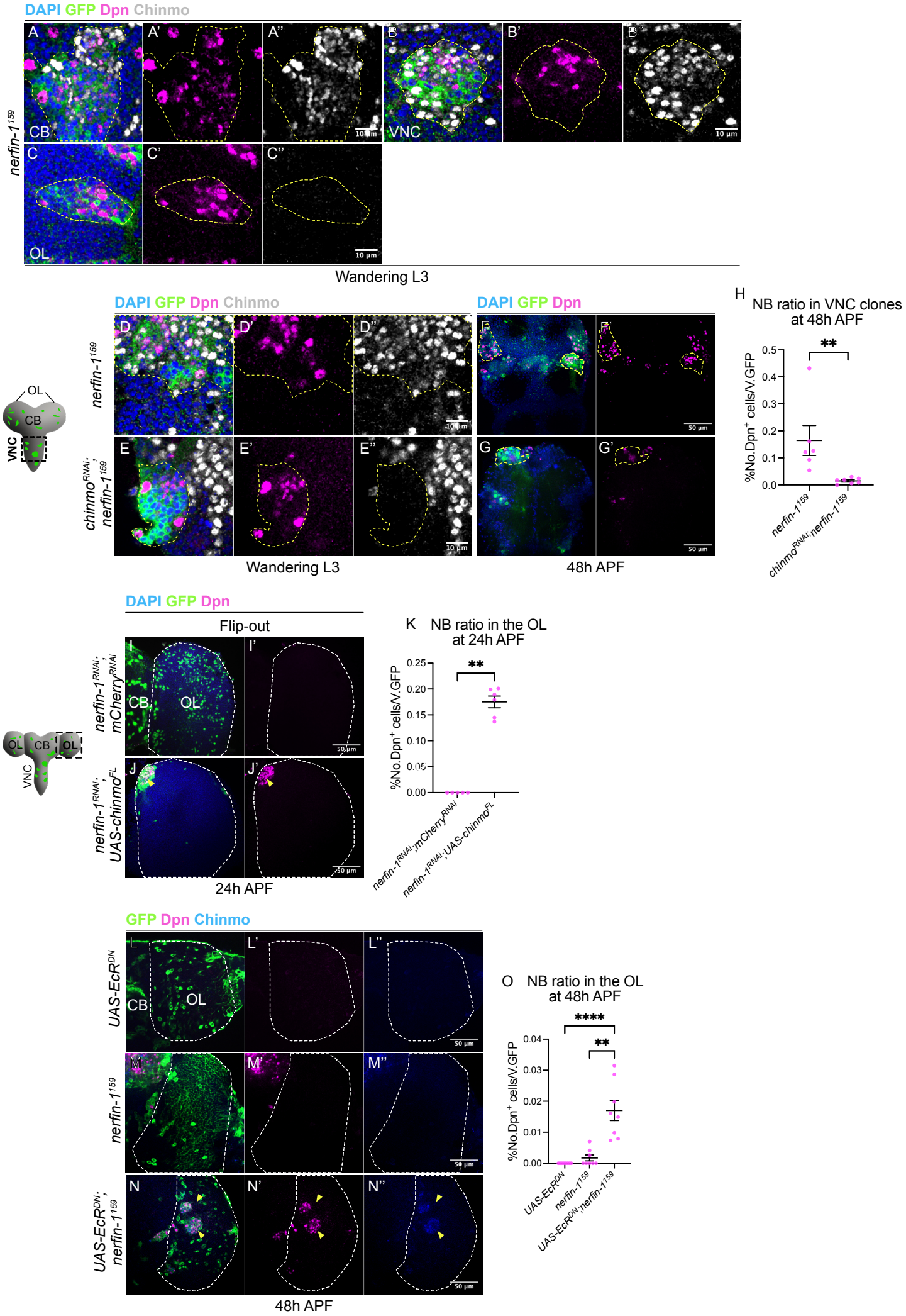
DAPI GFP Dpn Chinmo
nerfin-1159
A
A'
A''
B
B'
B''
CB
VNC
C
C'
C''
OL
10 µm
Wandering L3
DAPI GFP Dpn Chinmo
DAPI GFP Dpn
D
D'
D''
E
E'
E''
F
F'
G
G'
chinmoRNAi; nerfin-1159
50 µm
Wandering L3
48h APF
H
NB ratio in VNC clones at 48h APF
%No.Dpn+ cells/V.GFP
**
nerfin-1159
chinmoRNAi;nerfin-1159
DAPI GFP Dpn
Flip-out
I
I'
J
J'
nerfin-1RNAi; mCherryRNAi
nerfin-1RNAi; UAS-chinmoFL
24h APF
K
NB ratio in the OL at 24h APF
nerfin-1RNAi;mCherryRNAi
nerfin-1RNAi;UAS-chinmoFL
GFP Dpn Chinmo
L
L'
L''
M
M'
M''
N
N'
N''
UAS-EcRDN
UAS-EcRDN; nerfin-1159
48h APF
O
NB ratio in the OL at 48h APF
****
UAS-EcRDN
UAS-EcRDN;nerfin-1159

The steroid hormone ecdysone is a central regulator of developmental transitions in insects including *Drosophila* (Thummel, 2001). In the wildtype CNS, it has been previously shown that ecdysone signalling activation at the critical weight (mid-L3 stage) is required to repress Chinmo transcription specifically in the OL but not the CB/VNC (Dillard et al., 2018). Therefore, it is plausible that ecdysone signalling inhibits Chinmo expression in *nerfin-1*^{159} dedifferentiated NBs in the OL akin to the developmental context. At 48 hrs APF, we found that Ecdysone Receptor (EcR) is expressed in *nerfin-1*^{159} clones at a similar level to the surrounding WT cells in both the OL and VNC (Supplementary Figure 2C-D). This suggest that *nerfin-1*^{159} dedifferentiated NBs can respond to ecdysone signals in all brain regions. To test the role of ecdysone signalling in the suppression of Chinmo, we expressed a dominant negative form of EcR (EcR^{DN}) (Sieber & Spradling, 2015) in *nerfin-1*^{159} clones. *UAS-EcR*^{DN} expression alone was neither sufficient to derepress Chinmo nor promote the persistence of NBs in the OL at 48 hrs APF (Figure 3L, O). Nevertheless, *UAS-EcR*^{DN} expression in *nerfin-1*^{159} clones caused Chinmo to be upregulated, accompanied by increased NB persistence in the pupal OL compared to *UAS-EcR*^{DN} and *nerfin-1*^{159} control clones (Figure 3L-O). Altogether, these suggest that ecdysone signalling is necessary to silence Chinmo in *nerfin-1*^{159} clones in the pupal OL, causing the dedifferentiated NBs to lose tumorigenicity and differentiate.

Lola and Nerfin-1 have different expression patterns and regulate different gene sets in the developing OL medulla

lola loss-of-function (*lola*^{E76} – a null mutation where all Lola isoforms (Goeke et al. 2003) are deleted) causes neuronal dedifferentiation and consequently, tumour formation specifically in the adult OL (Southall et al., 2014). Indeed, we observed ectopic NB formation in *lola*^{E76} clones in the deep section of the OL at wandering L3 stage, indicating neuronal dedifferentiation (Figure 4A). However, only a subset of cells in the clones expressed the NB marker Dpn, suggesting that the clone is heterogeneous. At 48 hrs APF, *lola*^{E76} clones contained multiple Dpn^{+} ectopic NBs in the OL as well as many PH3^{+} cells (Figure 4B-C). As such, it is likely that these NBs were capable of proliferation beyond the normal period of neurogenesis. Noteworthy, we found that some of the cells within *lola*^{E76} clones was able to undergo differentiation, as indicated by the presence of neuronal marker Elav and glial marker Repo at 48 hrs APF (Supplementary Figure 3A-A'''). Collectively, these data suggest that beyond region-specific mechanisms, the ability to form tumours is also determined by the nature of the genetic mutations; while *nerfin-1*^{159} dedifferentiated NBs are eliminated, *lola*^{E76} dedifferentiated NBs remain proliferative to initiate tumorigenesis in the pupal OL.

As tumours generated via the loss-of-function of *nerfin-1* and *lola* caused distinct outcomes in the OL, we hypothesized that Nerfin-1 and Lola regulate different sets of target genes during medulla neurogenesis. To test this hypothesis, we first characterised the expression pattern of Nerfin-1 and Lola

Figure 4

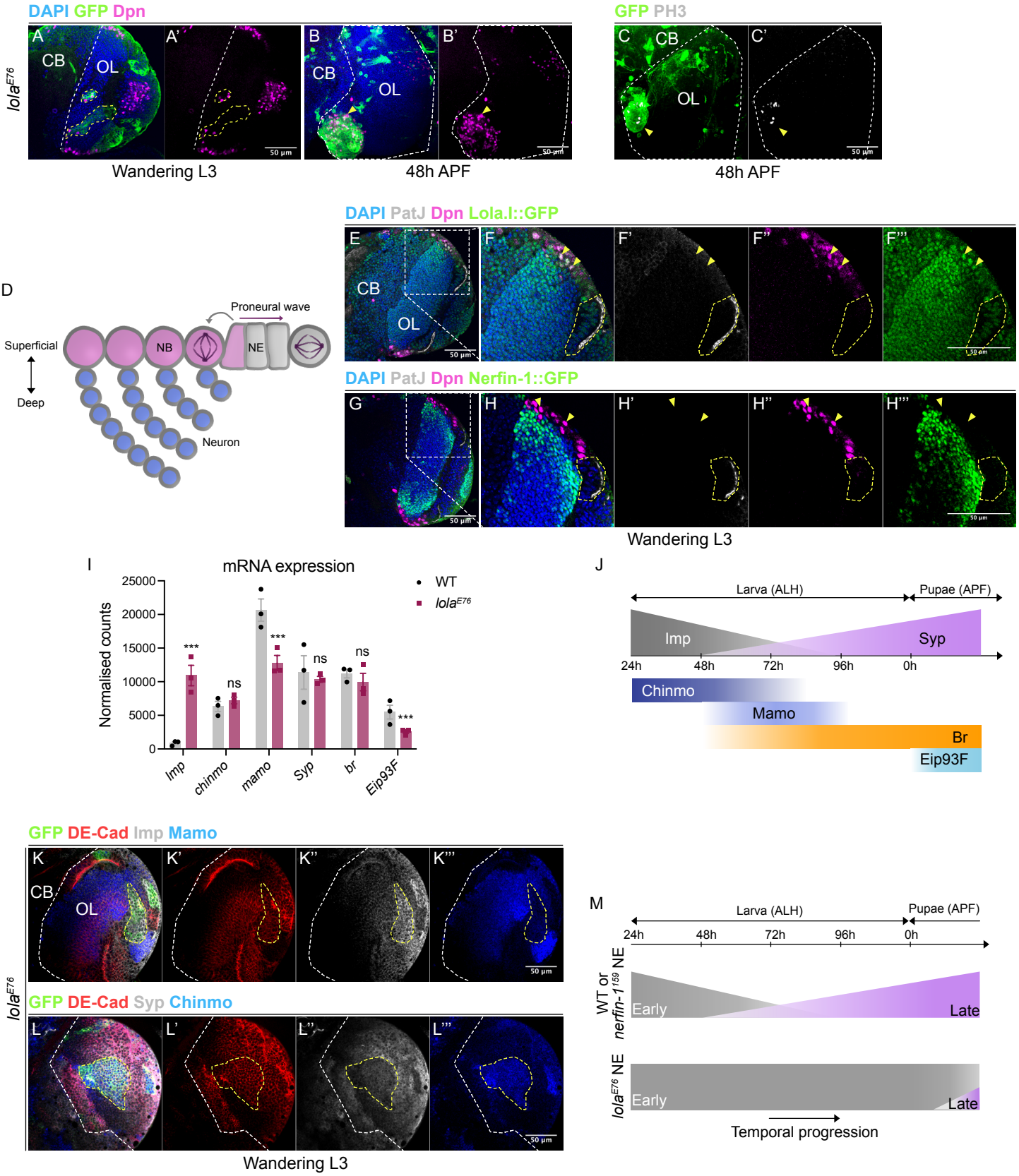
DAPI GFP Dpn
lola^E76
A
A'
CB
OL
B
B'
Wandering L3
48h APF
GFP PH3
C
C'
48h APF
DAPI PatJ Dpn Lola.I::GFP
E
F
F'
F''
F'''
DAPI PatJ Dpn Nerfin-1::GFP
G
H
H'
H''
H'''
Wandering L3
D
Proneural wave
Superficial
Deep
NB
NE
Neuron
I
mRNA expression
Normalised counts
WT
lola^E76
Imp
chinmo
mamo
Syp
br
Eip93F
ns
***
J
Larva (ALH)
Pupae (APF)
Imp
Syp
24h
48h
72h
96h
0h
Chinmo
Mamo
Br
Eip93F
GFP DE-Cad Imp Mamo
K
K'
K''
K'''
GFP DE-Cad Syp Chinmo
L
L'
L''
L'''
Wandering L3
M
Larva (ALH)
Pupae (APF)
24h
48h
72h
96h
0h
WT or nerfin-1^159 NE
lola^E76 NE
Early
Late
Temporal progression

using their respective GFP reporters in the OL at wandering L3 stage. From mid-larval stages, medulla NBs located on the cortical surface are generated from a pseudostratified neuroepithelium (NE) in the OL (Egger et al., 2007; Yasugi et al., 2008) (Figure 4D). Upon NE-NB transition, each NB then divides asymmetrically multiple times to self-renew and to generate ganglion mother cells (GMCs), which in turn divide once to produce medulla neurons. The neuronal progeny of each NB forms a chain, with newly generated neurons occupying the most superficial position close to the NBs and GMCs, and the oldest neurons occupying the deepest layer. We stained the larval brains for PatJ to mark the apical membrane of NE cells and Dpn to mark the NBs. For Lola, we used a GFP against Lola isoform I (Lola.I::GFP) which was previously shown to be expressed in the NBs and neurons of the larval OLs (H. Zhu et al., 2022). We observed that Lola.I::GFP was expressed in the nuclei of $PatJ^{+}$ NE cells (Figure 4E-F, yellow dash lines) and Dpn^{+} NBs (Figrue 4E-F, arrowheads). Conversely, Nerfin-1::GFP was not expressed in the NE (Figure 4G-H, yellow dash lines) and majority of the NBs (Figure 4G-H, arrowheads). Together, these data suggest that Lola and Nerfin-1 are likely required to function in different cell types in the developing OL medulla.

To explore target genes downstream of Lola and Nerfin-1, we performed bulk RNA-sequencing and compared the transcriptional profiles of *lola*^{E76}, *nerfin-1*^{159}, and wildtype (WT) clones from the OLs of wandering L3 larva. Multidimensional plot showed good clustering of samples according to clone genotypes, indicating strong similarities within groups and clear separation between conditions (Supplementary Figure 3B). Thus, the major source of variation in the RNA-seq data is driven by genetic mutations (*lola*^{E76}, *nerfin-1*^{159}, or wildtype), supporting the quality and reproducibility of our data. Differential expression analyses (adjusted p-value<0.05; log(fold-change), logFC>0.58) revealed 94 differentially expressed genes, including 65 upregulated and 29 downregulated genes in *lola*^{E76} compared to WT clones. Between *nerfin-1*^{159} and WT clones, there were 164 differentially expressed genes, including 80 upregulated and 82 downregulated genes. Notably, only 11 genes were shared between *lola*^{E76} versus WT and *nerfin-1*^{159} versus WT comparisons (Supplementary Figure 3C). Intriguingly, between *lola*^{E76} and WT clones, gene ontology (GO) enrichment for upregulated genes included terms involved in the digestive tract and muscle development (Supplementary Figure 3D). These unexpected results suggest that Lola may play a role in suppressing non-CNS genes to ensure the faithfulness of neural identity. Whereas GO enrichment for downregulated genes included synaptic transmission and membrane potential (Supplementary Figure 3D), indicating that Lola promotes genes required for neuronal maturation. GO terms enriched for genes upregulated in *nerfin-1*^{159} clones included NB division and proliferation (Supplementary Figure 3E). GO terms enriched for genes downregulated included terms involved in regulation of synaptic transmission and membrane potential (Supplementary Figure 3E). Therefore, Nerfin-1 appears to govern neuronal cell fate maintenance by inhibiting self-renewal and proliferation genes while promoting neuronal maturation. Taken together,

our data suggest that Lola and Nerfin-1 have different expression patterns and target different sets of genes with minimal overlap in the developing medulla.

Lola but not Nerfin-1 promotes timely progression of the temporal series in the NE

Since we and others have demonstrated that Lola is expressed in the medulla NE (Figure 4E-F) (H. Zhu et al., 2022), we next investigated its function in this cell population. Interestingly, our RNA-seq data showed that *Imp*, *mamo* and *Eip93F* levels were significantly altered in *lola*^{E76} compared to WT clones (Figure 4I). In particular, *Imp* was upregulated (logFC=3.74) whilst *mamo* and *Eip93F* were downregulated (logFC=0.64 and 1.04, respectively). NE cells express a series of temporal factors consisted of Imp, Chinmo, Mamo, Syp, Br and Eip93F that are then inherited by their progenies (Arain et al., 2022). Imp and Chinmo mark the early temporal window whilst Syp, Br, and Eip93F mark the late temporal window (Figure 4J). In addition to RNA-seq data, our immunostaining showed that *lola*^{E76} NE cells (marked by DE-Cadherin (DE-Cad)) exhibited an upregulation of Imp and Chinmo compared to WT cells outside of the clones at wandering L3 stage (Figure 4K-L). Conversely, Mamo and Syp were downregulated in *lola*^{E76} NE cells compared to wildtype cells (Figure 4K-L), suggesting that the early temporal window in the NE was extended at the expense of the late temporal window. In *nerfin-1*^{159} NE cells, the expression of Imp, Chinmo, Syp, and Mamo did not appear altered compared to surrounding wildtype counterparts (Supplementary Figure 3F-G). Altogether, our results suggest that only Lola, but not Nerfin-1 is required for the progression of the temporal series in the NE (Figure 4M).

Chinmo and Imp promote the persistence of *lola*^{E76} dedifferentiated NBs in the pupal OL

As Chinmo is the key determinant that sustains dedifferentiated NB proliferation during pupal life in *nerfin-1*^{159} clones, we next examined Chinmo expression in *lola*^{E76} clones at wandering L3 stage. We found that *lola*^{E76} clones expressed high levels of Chinmo in the OL (Figure 5A-A”). To assess whether Chinmo upregulation is functionally required to promote the persistence of *lola*^{E76} dedifferentiated NBs in the pupal OL, we knocked down Chinmo in *lola*^{E76} clones. This manipulation sufficiently reduced Chinmo expression at wandering L3 stage (Figure 5B-B”). At 48 hrs APF, Chinmo knockdown caused a significant reduction in the NB ratio the OL, and a dispersion of mutant cells, indicating neuronal differentiation (Morante et al., 2011) (Figure 5C-D, F). In addition to Chinmo, the RNA-binding protein Imp and Lin-28 is other components of the oncogenic module that defines the oncogenic competency of dedifferentiated NBs in the VNC (Narbonne-Reveau et al., 2016). In our RNA-seq data, we found that differentially upregulated genes in *lola*^{E76} cells included both *Imp* and *lin-28* with logFC of 3.74 and 6.20, respectively. Moreover, Imp knockdown in *lola*^{E76} clones significantly reduced the persistence

Figure 5

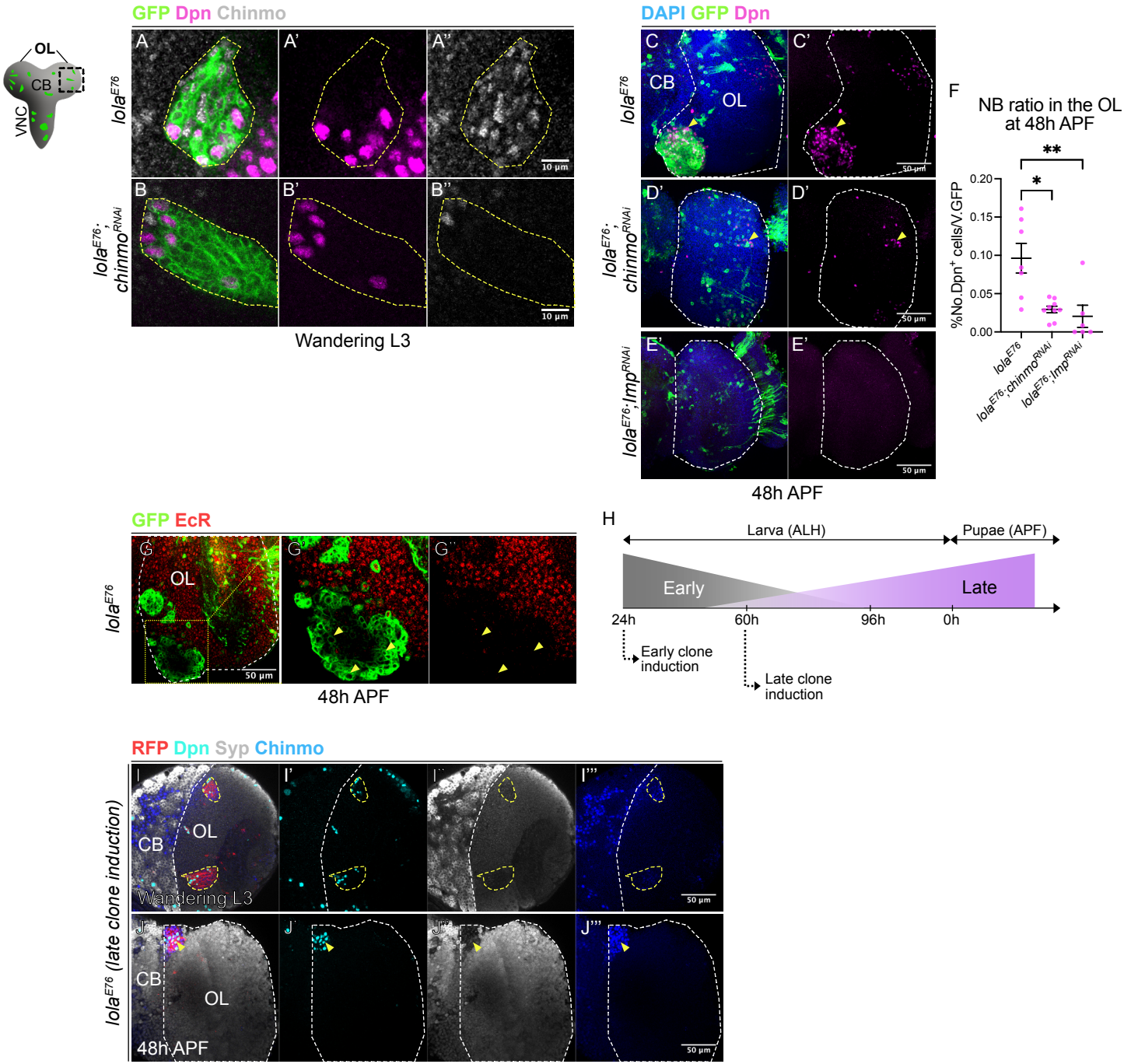
GFP Dpn Chinmo
OL
CB
VNC
lola^E76
lola^E76; chinmo^RNAi
A
A'
A''
B
B'
B''
10 µm
Wandering L3
DAPI GFP Dpn
C
C'
CB
OL
D'
E'
lola^E76; Imp^RNAi
50 µm
48h APF
F
NB ratio in the OL at 48h APF
%No.Dpn+ cells/V.GFP
0.20
0.15
0.10
0.05
0.00
*
**
lola^E76
lola^E76;chinmo^RNAi
lola^E76;Imp^RNAi
GFP EcR
G
G'
G''
H
Larva (ALH)
Pupae (APF)
Early
Late
24h
60h
96h
0h
Early clone induction
Late clone induction
RFP Dpn Syp Chinmo
I
I'
I''
I'''
J
J'
J''
J'''
lola^E76 (late clone induction)
Wandering L3
48h APF

307 of NBs in *lola*^{E76} clones at 48h APF, similar to Chinmo knockdown (Figure 5D-F). Thus, Chinmo and
308 Imp are required to sustain *lola*^{E76} dedifferentiated NBs in the pupal OL.

309

310 **Chinmo upregulation occurs independently of ecdysone and the temporal identity of its cell-of-**
311 **origin upon Lola inactivation**

312 We next aimed to understand how Chinmo is regulated in *lola*^{E76} clones. As ecdysone signalling
313 necessitates the silencing of Chinmo to eliminate *nerfin-1*^{159}dedifferentiated NBs specifically in the OL,
314 we wondered how *lola*^{E76} dedifferentiated NBs were able to maintain Chinmo expression despite its
315 location in the OL. Interestingly, we found that EcR expression was downregulated in *lola*^{E76} clones
316 compared to wildtype surrounding cells in the OL at 48 hrs APF (Figure 5G-G'', arrowheads). As such,
317 it is likely that *lola*^{E76} dedifferentiated NBs in the OL are not receptive to ecdysone signals that normally
318 inhibits *chinmo*, at least during pupal development.

319 We have shown that Lola promotes the Imp^{+}Chinmo^{+} early temporal identity in the NE. As NBs
320 and neurons inherit their temporal identity from the NE progenitors, it is possible that *lola*^{E76}
321 dedifferentiated NBs express Chinmo because they are generated during the Chinmo^{+} time window (24
322 hrs ALH, early time point, Figure 5H). To test this postulation, we induced *lola*^{E76} clones that bypass
323 the Chinmo^{+} time window (60 hrs ALH, late time point, Figure 5H). Despite being generated in the
324 Chinmo^{-} time window, late induced *lola*^{E76} clones continued to express the early temporal marker
325 Chinmo and failed to turn on the late temporal marker Syp at wandering L3 stage (Figure 5I-I'''). At 48
326 hrs APF, *lola*^{E76} ectopic NBs persisted in the OL (Figure 5J-J''', arrowheads). Thus, our data suggest
327 that the persistence of *lola*^{E76} dedifferentiated NBs is independent of whether they were generated
328 during the Chinmo^{+} or Chinmo^{-} temporal window.

329 We also attempted to test if inhibiting the early temporal identity in the NE can prevent the
330 persistence of *lola*^{E76} dedifferentiated NBs in the pupal OL. To do so, we overexpressed Syp in *lola*^{E76}
331 clones, which was shown to repress the expression of early tTFs such as Chinmo and Imp in the
332 CB/VNC (Liu et al., 2015; Ren et al., 2017; Yang et al., 2017). However, we found that at 48 hrs APF,
333 Syp overexpression was insufficient to downregulate Imp and eliminate *lola*^{E76} ectopic NBs in the OL
334 (Supplementary Figure 4A-C). Thus, the regulatory relationship between Imp-Chinmo-Syp in the OL
335 likely differs from that in the CB/VNC.

336

337 **Notch signalling is not required for neuronal dedifferentiation in *lola*^{E76} clones**

338 We and others previously showed that neuronal dedifferentiation induced via *nerfin-1* loss-of-function
339 in the OL requires Notch signalling activation (Vissers et al., 2018; Xu et al., 2017). We wondered if

340 Notch signalling is also required for neuronal dedifferentiation induced by *lola* loss-of-function. Our
341 RNA-seq data showed that while *Notch* (*N*) was upregulated (logFC=0.88) in *lola*^{E76} compared to WT
342 clones, *Delta* which encodes for a Notch ligand, as well as the downstream effector of Notch signalling,
343 *E(spl)mγ* were not significantly altered (Supplementary Figure 4D). In line with this, our
344 immunostaining showed that the intracellular domain of Notch (NICD) was upregulated in *lola*^{E76}
345 clones whereas Delta appeared unaltered compared to WT cells outside of the clones in the OL at
346 wandering L3 stage (Supplementary Figure 4E-F). To address if Notch signalling is necessary for
347 neuronal dedifferentiation induced via *lola* loss-of-function, we knocked down *Notch* by RNAi in
348 *lola*^{E76} clones. This manipulation did not significantly alter the rate of dedifferentiation at wandering
349 L3 stage compared to the *lola*^{E76} control (Supplementary Figure 4G-I). Together, our data suggest that
350 Notch signalling does not mediate neuronal dedifferentiation derived from Lola inactivation.

351

352 **_lola_^{E76} dedifferentiated NBs exhibited delayed temporal progression in the OL**

353 Previous studies have shown that medulla NBs sequentially express a series of tTFs including
354 Homothorax (Hth), Eyeless (Ey), Sloppy paired (Slp), Dichaete (D), and Tailless (Tll) as they age (Li
355 et al., 2013) (Figure 6A). Thus, we next aimed to investigate whether this temporal series is altered in
356 *lola*^{E76} dedifferentiated NBs using three representatives: the early-tTF Ey, mid-tTF Slp and late-tTF Tll
357 to assay for temporal progression. It was previously shown that *lola* knockdown in medulla NBs caused
358 delayed temporal progression during late larval stages (H. Zhu et al., 2022). Consistent with this, at
359 wandering L3 stage, we observed that Ey, Slp, and Tll expression appeared reduced in *lola*^{E76} NBs
360 compared to the WT counterparts on the superficial layers, indicative of a delayed temporal progression
361 (Figure 6B-F). Our results therefore confirm the role of Lola in controlling the speed of temporal
362 progression in the medulla NBs. In the deep layers of the larval medulla where *lola*^{E76} dedifferentiated
363 NBs are located, we observed that a subset of cells in *lola*^{E76} clones expressed Ey and Slp, but not Tll
364 at wandering L3 stage (Figure 6B, G-H, K). By 48 hrs APF, fewer dedifferentiated NBs expressed Ey
365 and Slp, and more cells expressed Tll in *lola*^{E76} clones (Figure 6I-K). Altogether, our data suggest that
366 *lola*^{E76} dedifferentiated NBs exhibited delayed progression through the temporal series (Figure 6L).

367

368 **Lola expression in _nerfin-1_ loss-of-function clones promotes the elimination of dedifferentiated**
369 **NBs in the OL**

370 Given that both Nerfin-1 and Lola are required to maintain the differentiated state of medulla neurons,
371 we wondered if these factors acted redundantly. To examine this, we assessed the expression of
372 Lola.I::GFP reporter in *nerfin-1*^{RNAi} flip-out clones at wandering L3 stage. Our immunostaining showed
373 that Lola.I::GFP expression was similar between *nerfin-1*^{RNAi} clones and WT cells in the medulla (Figure

Figure 6

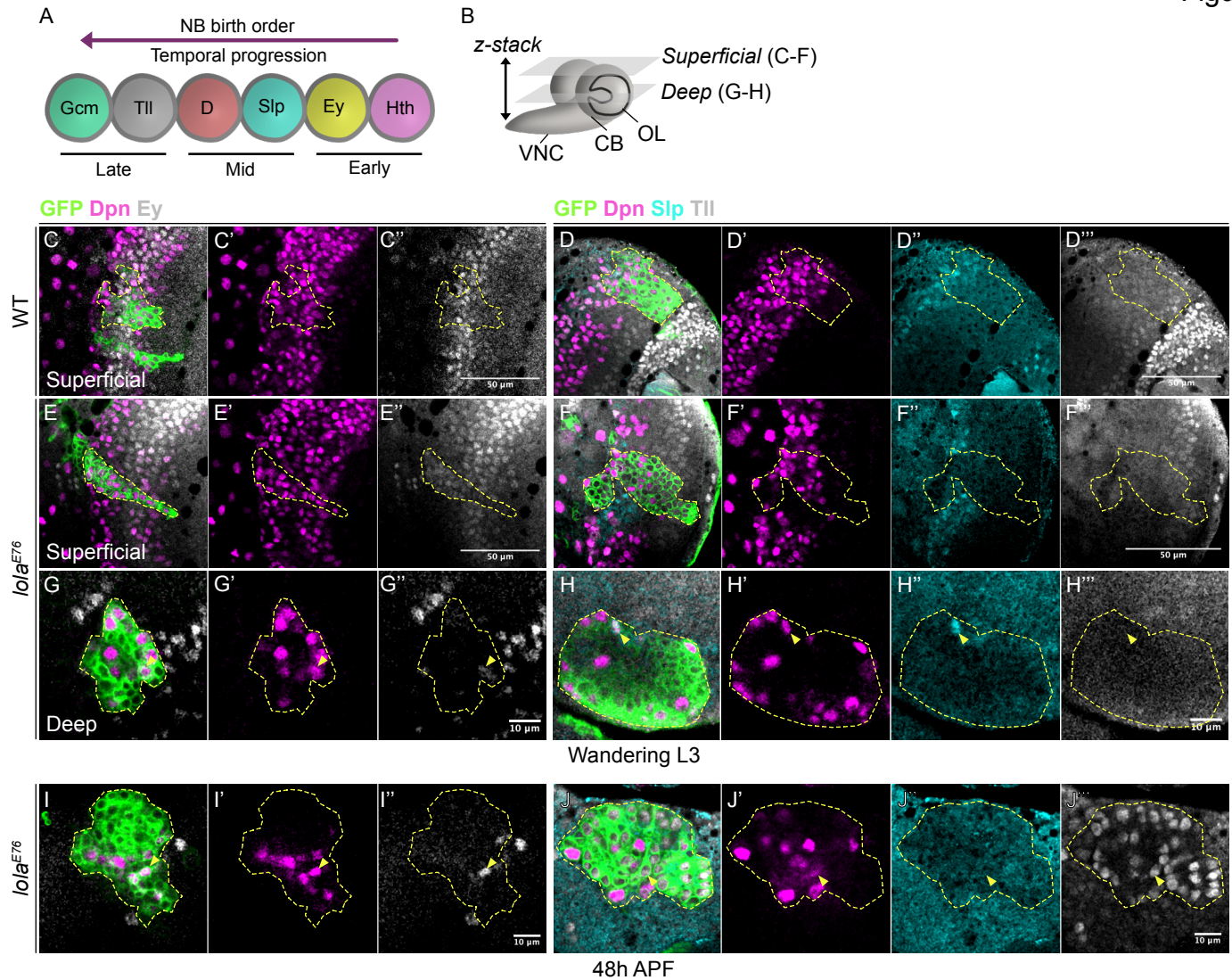
A
NB birth order
Temporal progression
Gcm
Tll
D
Slp
Ey
Hth
Late
Mid
Early
B
z-stack
Superficial (C-F)
Deep (G-H)
VNC
CB
OL
GFP Dpn Ey
GFP Dpn Slp Tll
WT
lolaE76
Superficial
Deep
50 µm
10 µm
Wandering L3
48h APF

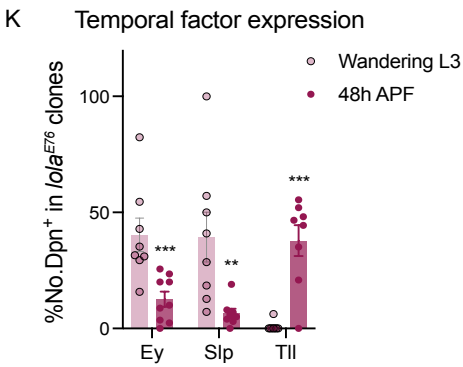
K
Temporal factor expression
Wandering L3
48h APF
%No.Dpn+ in lolaE76 clones
100
50
0
***
**
***
Ey
Slp
Tll

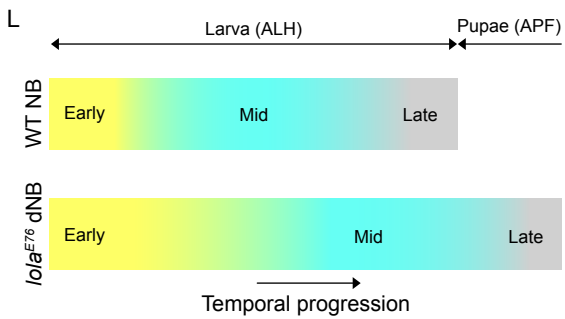
L
Larva (ALH)
Pupae (APF)
WT NB
Early
Mid
Late
lolaE76 dNB
Early
Mid
Late
Temporal progression

374 7A). Similarly, *lola* mRNA expression level was not significantly altered in *nerfin-1*^{159} compared to WT
375 clones (Figure 7B). To test if Lola is functionally required in *nerfin-1*^{159} dedifferentiated NBs, we
376 knocked down Lola in *nerfin-1*^{159} clones by RNAi. In *nerfin-1*^{159}, *lola*^{RNAi}, and *lola*^{RNAi};*nerfin-1*^{159}
377 clones, we observed ectopic NBs in the deep layers of the medulla at wandering L3 stage (Figure 1C,
378 7C-D), indicative of neuronal dedifferentiation. By 48 hrs APF, *lola*^{RNAi} *and lola*^{RNAi};*nerfin-1*^{159} clones,
379 but not *nerfin-1*^{159} clones displayed persistent ectopic NBs in the OLs (Figure 1E, 7E-F). Notably,
380 quantifications showed that the NB ratio of *lola*^{RNAi};*nerfin-1*^{159} clones in the OL was significantly higher
381 than that of *lola*^{RNAi} clones at 48 hrs APF (Figure 7G). Collectively, our results suggest that Lola
382 promotes the elimination of dedifferentiated NBs in *nerfin-1* loss-of-function clones in the OL during
383 pupal development.

384

385 **Discussion**

386 Dedifferentiation of mature specialised cells into stem-progenitor cells that can self-renew and re-
387 differentiate provides a valuable mean for tissue regeneration. However, studies have shown that
388 dedifferentiation is a source of cancer stem cells that can drive malignant tumour overgrowth and
389 heterogeneity (Friedmann-Morvinski & Verma, 2014). Thus, it is crucial to understand how these
390 distinct outcomes of dedifferentiation are specified. In this work, we have discovered that oncogenic
391 tTFs are key determinants of this process. In the CB/VNC, *nerfin-1*^{159} dedifferentiated NBs express the
392 oncogenic tTF Chinmo that promotes their persistence during pupal development. Conversely, in the
393 OL, ecdysone signalling promotes *chinmo* silencing. The absence of Chinmo ensures the elimination
394 of *nerfin-1*^{159} dedifferentiated NBs via two mechanisms: apoptosis and terminal differentiation. *lola*^{E76}
395 dedifferentiated NBs on the other hand are likely not responsive to ecdysone signals during pupal
396 development, thereby can persist in the pupal OL due to the persistence of Chinmo. Together, these
397 mechanisms determine the distinct outcome of neuronal dedifferentiation between different regions of
398 the brain, as well as the differential consequences of dedifferentiation caused by *nerfin-1* vs. *lola* loss-
399 of-function (Figure 7H). Together, our data offers evidence that region-specific cues as well as genetic
400 mutations can contribute to the oncogenic competence of stem-progenitor cells derived from
401 dedifferentiation.

402 **Chinmo is the key determinant of oncogenic competence in the CNS**

403 Our data suggest that the differential expression and regulatory mechanism of Chinmo can dictate the
404 oncogenic outcome of dedifferentiated NBs; such that high Chinmo induces oncogenesis whilst no/low
405 Chinmo allows the elimination of the dedifferentiated progenitor pool. An outstanding question that
406 remains to be addressed is the mode-of-action of Chinmo. In the wildtype CB/VNC, Chinmo acts as a
407 tTF that defines the early temporal window in the NBs and their progenies, but not a regulator of NB
408 proliferation (Maurange et al., 2008; Narbonne-Reveau et al., 2016). In *pros*$^{-/-}$ dedifferentiated tumours

Figure 7

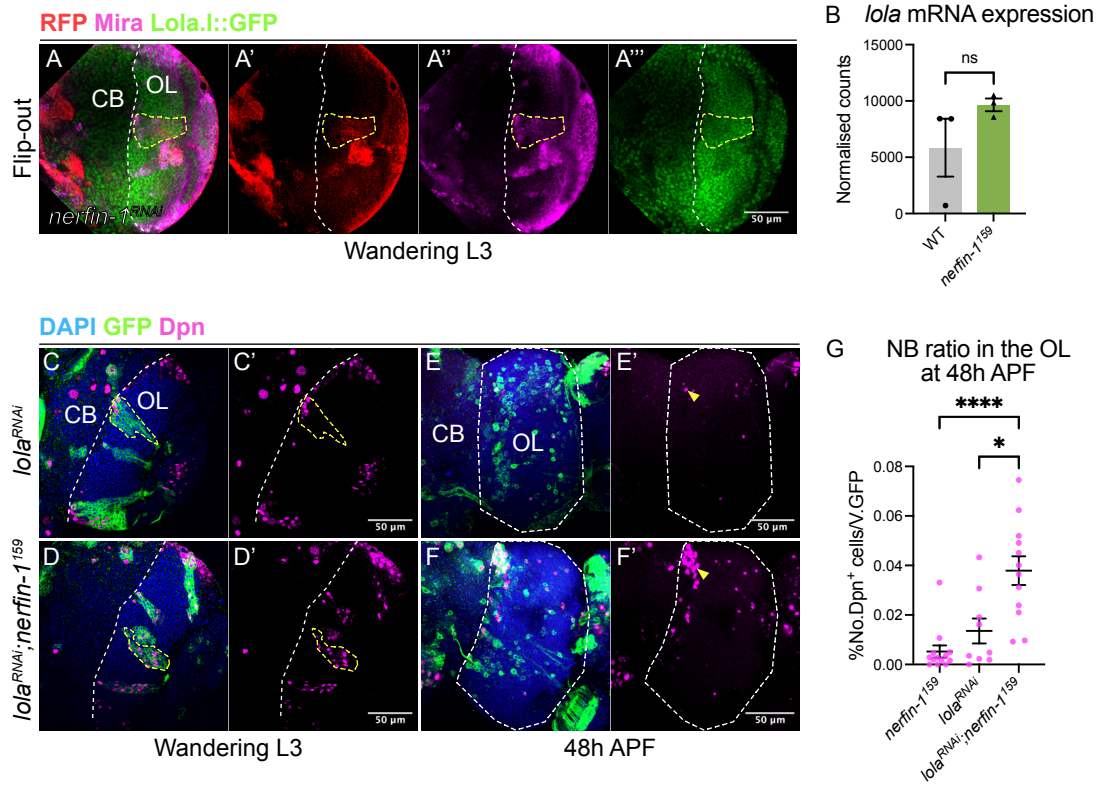
RFP Mira Lola.I::GFP
Flip-out
A
A'
A''
A'''
CB
OL
nerfin-1RNAi
50 µm
Wandering L3
B
lola mRNA expression
Normalised counts
15000
10000
5000
0
ns
WT
nerfin-1159
DAPI GFP Dpn
lolaRNAi
lolaRNAi;nerfin-1159
C
C'
D
D'
E
E'
F
F'
Wandering L3
48h APF
G
NB ratio in the OL at 48h APF
%No.Dpn+ cells/V.GFP
0.08
0.06
0.04
0.02
0.00
****
*
nerfin-1159
lolaRNAi
lolaRNAi;nerfin-1159

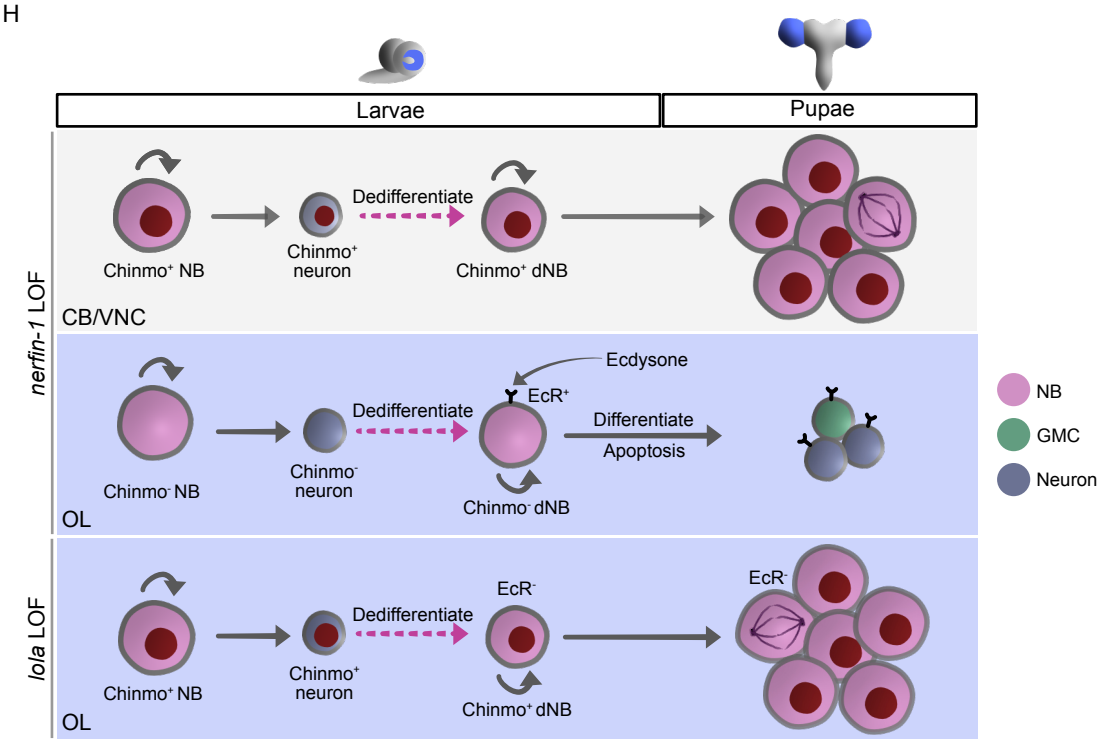
H
Larvae
Pupae
nerfin-1 LOF
Chinmo+ NB
Chinmo+ neuron
Dedifferentiate
Chinmo+ dNB
CB/VNC
Ecdysone
EcR+
Dedifferentiate
Differentiate
Apoptosis
Chinmo- NB
Chinmo- neuron
Chinmo- dNB
OL
lola LOF
Chinmo+ NB
Chinmo+ neuron
Dedifferentiate
EcR-
Chinmo+ dNB
EcR-
OL
NB
GMC
Neuron

409 in the VNC, Chinmo was suggested to promote cell division and protein synthesis (Narbonne-Reveau
410 et al., 2016). However, in the OL, Chinmo does not only act as a tTF in the NE progenitors and its
411 progeny but also governs NE cell self-renewal, and thereby, the timing of NE-NB transition (Dillard et
412 al., 2018). Therefore, how the function of Chinmo differs between the CB/VNC and the OL needs
413 further investigation.

414 **Pupal steroid hormone signalling promotes elimination of dedifferentiated NBs by suppressing**
415 **oncogenic tTFs**

416 Our data showed that inhibiting ecdysone signalling promotes ectopic Chinmo expression in *nerfin-1*$^{-/-}$
417 dedifferentiated NBs in the pupal OL (Figure 3L-O). Therefore, ecdysone signals during pupal
418 development are required to suppress Chinmo expression in *nerfin-1*$^{-/-}$ clones. This is consistent with
419 previous reports, where it was shown that Chinmo expression is silenced in the NE by a pulse of
420 ecdysone at the critical weight (Dillard et al., 2018a). This peak of ecdysone coincides with the
421 acceleration of the NE-NB transition, followed by post-embryonic neurogenesis in the medulla (Lanet
422 et al., 2013). As such, most medulla neurons are generated post-critical weight. In addition, they are
423 Chinmo-negative and thus incompetent to initiate tumour overgrowth following dedifferentiation.
424 However, because *nerfin-1*$^{-/-}$ clones were induced during the early Chinmo^{+} temporal window of the
425 medulla, it was surprising that the dedifferentiated NBs did not inherit Chinmo from the NE.

426 Nevertheless, it remains to be addressed whether ecdysone signalling is required for the
427 initiation and/or the maintenance of Chinmo silencing in this case. In the developing medulla, ecdysone
428 signalling at the mid-larval stage induces expression of its target gene *br* in the NE to promote the NE-
429 NB transition (Y. Zhou et al., 2019a). In the wing imaginal disc, ecdysone signalling induces a Chinmo-
430 to-Br expression switch during late larval stage (Narbonne-Reveau & Maurange, 2019). In addition, Br
431 and Chinmo have been shown to inhibit each other's expression (Chafino et al., 2023; Narbonne-Reveau
432 & Maurange, 2019). As such, it is possible that like the wing disc, ecdysone signalling inhibits Chinmo
433 expression in the *nerfin-1*$^{-/-}$ dedifferentiated NBs via its downstream effector Br.

434 In the wildtype CB/VNC, it was previously shown that ecdysone signalling is dispensable for
435 Chinmo expression in the NBs (Dillard et al., 2018a), which may account for the persistence of the
436 *nerfin-1*$^{-/-}$ dedifferentiated NBs in these regions. Lola inactivation was previously shown to cause
437 neuronal dedifferentiation only in OL (Southall et al., 2014). Here, we found that *lola*$^{-/-}$ dedifferentiated
438 NBs in the OLs continued to divide into late pupal stages (Figure 4B-C, and as reported in Southall et
439 al., 2014). Moreover, we found that *lola*$^{-/-}$ clones in the OL are likely not receptive to ecdysone because
440 they do not express EcR (Figure 5G). This may account for Chinmo expression in *lola*$^{-/-}$ clones in the
441 OL which in turn drives the persistence of dedifferentiated NBs. However, it is so far unclear how Lola
442 regulates EcR expression.

443 **Differential target genes of Nerfin-1 and Lola in the developing medulla**

Our RNA-seq analyses have revealed that there is very little overlap between differential expressed genes in *nerfin-1*$^{-/-}$ and *lola*$^{-/-}$ clones compared to the wildtype (Supplementary Figure 3C). This may account for the contrasting tumorigenic phenotype between two mutations in the OL. The differentially expressed genes are enriched in partially overlapping GO terms, in both cases, GO enrichment for downregulated genes involves neuronal function and maturation (Supplementary Figure 3D-E). In *nerfin-1*$^{-/-}$, GO enrichment for upregulated genes includes NB division and proliferation (Supplementary Figure 3E). This is expected given the expression pattern of Nerfin-1 in immature neurons in the developing medulla (Vissers et al., 2018; Xu et al., 2017). Interestingly, GO enrichment for upregulated genes in *lola*$^{-/-}$ clones are enriched in non-CNS genes (Supplementary Figure 3D). This echoes recent findings regarding the chromatin remodeller Mi-2 and the condensin I subunit Cap-G whose knockdowns in neurons cause ectopic upregulation of genes signatures of the fat body, the hindgut, or cilium assembly, etc, that tend to not associate with the CNS (Aughey et al., 2023; Hassan et al., 2020). Accordingly, it will be of interest to probe how Lola represses the expression of organ and lineage inappropriate genes in the neurons, either via chromatin remodelling or other mechanisms. Nevertheless, it is important to note that *lola*^{E76}-null mutation eliminates all 12 Lola isoforms (Goeke et al., 2003), preventing us from determining which specific isoform(s) knockdown is responsible for these unexpected results. Consequently, the role of individual Lola isoforms expressed in the medulla remains to be explored. Previous work showed that Lola-N overexpression can rescue tumour overgrowth caused by *lola*^{E76} dedifferentiated NBs in the adult OL (Southall et al., 2014). However, Lola-N mutant clones displayed no ectopic NBs in the adult OL (Dinges et al., 2017), suggesting that there is functional redundancy between Lola isoforms that also needs to be taken into consideration.

Another caveat in our study lies in the utilisation of bulk RNA-sequencing. As we and others have demonstrated that Nerfin-1 and Lola are expressed and function differently in different cell types of the developing medulla (Southall et al., 2014; H. Zhu et al., 2022), it is likely that bulk RNA-seq cannot capture the gene network dynamic as well as the heterogeneity with in *nerfin-1*$^{-/-}$ and *lola*$^{-/-}$ cells in all the lineages. Indeed, at wandering L3 stage, only a few cells expressed Dpn in *lola*^{E76} clones (Figure 4A), suggesting that our RNA-seq data is averaging the transcriptional outputs of the different cell states present in the mutant clones. This likely explains why upregulated genes in *lola*^{E76} clones were not enriched in GO terms involved in NB proliferation (Supplementary Figure 3D) (Southall et al., 2014).

Characterisations of paediatric brain tumours such as glioblastoma and medulloblastoma have revealed the link between the oncogenic mutations, the tumour location and the overall prognosis in patients (Gibson et al., 2010; Mackay et al., 2017; Sturm et al., 2012). In glioblastoma, two mutations of the *H3F3* gene that lead to two amino acid substitutions of the histone 3 variant 3, H3.3-G34R and H3.3-K27M induce tumour overgrowth in anatomical distinct regions of the CNS. While the H3.3-G34R subtype is mostly found in the brain hemisphere, the H3.3-K27M subtype is often found in the

hindbrain (Mackay et al., 2017; Sturm et al., 2012). A recent study using compartmentalised NSC culture derived from anatomical relevant areas showed that high expression of the transcription factor FOXG1 in the forebrain confers its housing NSCs the competency to undergo H3.3-G34R-induced oncogenic transformation (Bressan et al., 2021). Hence, differential gene expression profiles between brain regions appear to underpin their varying susceptibility to oncogenic transformation. Our investigation further suggests that elucidating the regionalised control of temporal patterning can aid us in understanding the outcome of dedifferentiated tumours; however, the result needs to be considered within the context of a specific mutation.

Materials and Methods

Fly stocks and husbandry

The fly strains utilised are detailed in the following table:

System	Genotype	Source
Flip-out	*hs-FLP,act>CD2>GAL4;UAS-Dcr2,UAS-GFP*	Lei Zhang
MARCM	*yw,hs-FLP;tub-GAL4,UAS-mCD8::GFP;FRT2A,tub-GAL80*	Alex Gould
	UAS-mCD8::GFP,hsFLP;FRT42D,tub-GAL80;tub-GAL4	Helena Richardson
	hs-FLP;FRT42D,tub-GAL80;tub-GAL4,UAS-mCD8::RFP	Kieran Harvey
	FRT42D,lola^{E76}	Tony Southall
	Df(3L)nerfin-1^{159}	Ward Odenwald
	FRT2A	Alex Gould
Reporter	*Nerfin-1::GFP*	BL67385
	Lola.I::GFP	BL38662
	UAS-mCherry-chinmo^{UTRs}	Cedric Maurange
RNAi	*UAS-pros RNAi*	BL42538
	UAS-gcm RNAi	VDRC110539
	UAS-chinmo RNAi (III)	BL33638
	UAS-chinmo RNAi (II)	This study
	UAS-EcR^{DN}	BL9451
	UAS-Imp RNAi	BL34977
	UAS-nerfin-1 RNAi	VDRC101631
	UAS-lola RNAi	VDRC101925
	UAS-mCherry RNAi	BL35784
	UAS-N RNAi	BL33611

Overexpression	*UAS-p35*	BL5072
	UAS-Myc	BL9674
	UAS-chinmo^{FL}	BL50740
	UAS-syp^{RB}::HA	Tzumin Lee
attP docking site	*P{CaryP}Msp300[attP40] (II)*	BL25709

Fly stocks were reared on standard media at 25ºC. For all experiments, embryos were collected overnight at either room temperature or 25ºC. For larval dissection, brains were dissected at wandering L3 stage. For pupal dissection, white pupae were selected and allowed to age to desired time points (24-48 hrs APF).

For clonal analysis, flip-out clos were induced at 24 hrs ALH, for 10 min at 37ºC then moved to 29ºC until dissection. This is except for experiments with *UAS-chinmo^{FL}* whereby clones were induced at 48 hrs ALH for 8 min and larva were allowed to develop until dissection at room temperature to prevent animal lethality. Mosaic Analysis with a Repressible Cell Marker (MACRM) (Lee & Luo, 1999) clones were induced at 24 hrs ALH unless indicated otherwise, for 30 min at 37ºC and then moved to 29ºC until dissection. This is except for experiments with *UAS-pros^{RNAi}* in which clones were induced for 15 min and animals were kept at 25ºC to prevent excessive tumour overgrowth in the CNS.

Generation of *UAS-chinmo^{RNAi}* (II) fly stock

To generate *chimmo^{RNAi}* fly stock, oligos were designed based on the *UAS-chinmo^{RNAi}* TRiP line (BL33638), with sense and anti-sense sequences as 5'-AGCGCGAATATCGTTGACAGA-3' and 5'-TCTGTCAACGATATTCGCGCT-3', respectively. After annealing, the resulting DNA fragment was cloned into VALIUM20 vector linearized by NheI and EcoRI. The ligation product was transformed into Stable Competent *E.Coli* (NEB C3040H). Transformed colonies were selected by the presence of pVALIUM20 vector by PCR with forward primer 5'-ACCAGCAACCAAGTAAATCAAC-3' and reverse primer 5'-TAATCGTGTGTGATGCCTACC-3'. Plasmids were purified from selected colonies using Isolate II Plasmid Miniprep (Meridian Bioscience) for sequencing and injected into flies carrying an attP40 docking site.

Immunostaining

Larval and pupal brains were dissected in phosphate buffered saline (PBS), fixed in 4% formaldehyde in PBS for 20 min and rinsed three times in 0.5% Triton X-100 in PBS (PBST) at room temperature. For immunostaining, brains were incubated in primary antibodies overnight at 4ºC, followed by two 0.5% PBST washes and then an overnight secondary antibody incubation at 4ºC. Brains were next washed twice with 0.5% PBST and optically cleared in 50% glycerol for 20 min. Samples were mounted

521 in either 80% glycerol or anti-fade mounting medium containing 4% n-propyl gallate, on glass slides
522 and sealed with coverslips (22x22 mm, No 1.5) for image acquisition. The primary antibodies were: rat
523 anti-Dpn (1:200, Abcam 195172), chick anti-GFP (1:1000, Abcam 13970), rat anti-Elav (1:50, DSHB
524 7E8A10), mouse anti-Repo (1:50, DSHB 8D12), rabbit anti-Dcp-1 (1:100, Cell Signalling 95785),
525 rabbit anti-Myc (1:100, Santa Cruz Biotech d-1-717), rabbit anti-RFP (1:200, Rockland #600-401-379),
526 mouse anti-Mira (1:100, a gift from Alex Gould), rabbit anti-PatJ (1:500, a gift from Helena
527 Richardson), rat anti-DE-Cad (1:200, DSHB DCAD2), rat anti-Chinmo (a gift from Nicholas Sokol),
528 guinea pig anti-Chinmo & rabbit anti-Syp & guine pig anti-Mamo (1:200, gifts from Claude Desplan),
529 mouse anti-EcR common (EcR^{comm}) (1:50, DSHB Ag10.2), rabbit anti-Imp (1:500, a gift from Paul M
530 Macdonald), mouse anti-NICD (1:50, DSHB C179C6), mouse anti-Delta (1:10, DSHB C5949B),
531 mouse anti-Ey (1:50, DSHB), guinea pig anti-Slp & rabbit anti-Tll (1:200, gifts from Kuniaki Saito).
532 Secondary donkey antibodies conjugated to Alexa 555, Alexa 647, goat antibodies conjugated to Alexa
533 405, 488, 555, and 647 (Molecular Probes and Abcam) were used at 1:500.

534

535 **Image acquisition and processing**

536 Images were acquired using Olympus FV3000 confocal microscope with 20X (NA 0.75, UPSALO) and
537 60X (NA 1.30, UPLSAPO) objectives. Δz=1.5 µm. Images were processed using Fiji
538 (https://imagej.net/Fiji). Quantification was performed in Fiji or via 3D reconstruction in Imaris
539 (Bitplane). To quantify the ratio of NBs or neurons in clones at the larval stage or in the pupal OL in
540 Imaris, GFP^+ volume were first detected and measured. The GFP^+ volume were then utilised to make a
541 mask for Dpn^+ cells or $Elav^+$ cells within the clones, which was in turn used to measure NB or neuron
542 numbers, respectively. The ratio of NBs or neurons in clones or in the OL were calculated as
543 $\%GFP^+Dpn^+$ or $\%GFP^+Elav^+$ cells in the total GFP^+ volume, respectively. Images were assembled in
544 Affinity Publisher 2. Schematics were created in Affinity Design 2. Scale bars = 10, 20, or 50 µm per
545 indicated in figures. Quantifications for the ratios of NBs expressing tTFs (Ey, Slp, and Tll) in $lola^{E76}$
546 clones were done manually in Fiji.

547

548 **RNA-sequencing**

549 *FRT42D* (wildtype), $FRT2A,nerfin\text{-}1^{159}$, $FRT42D,lola^{E76}$ mutant cells were isolated from wandering L3
550 stage OLs by FACS purification using previously published protocol (Harzer et al., 2013). Briefly, OLs
551 were dissected from the larval CNS in cold Schneider's culture medium (Gibco) and dissociated using
552 papain and collagenase I (Sigma-Aldrich). Cells were sorted by flow cytometry into lysis buffer and
553 extracted for RNA using Single cell purification kit (Norgen Biotek SKU51800). Samples from sorts
554 executed on different days were pooled into three samples per genotype, containing 33,000-105,000

cells (about 15-70 ng total RNA) per sample. RNA concentration and quality were analysed by Tapestation Bioanalyzer 4150. Libraries were amplified and prepared with QuantSeq (Lexogen) following standard protocol. RNA-sequencing was carried out on NextSeq2000 instrument (Illumina), using 100 base single-end reads and 100 cycles. RNA-seq samples consisted of three replicates per genotype and were all sequenced in the same batch.

Bioinformatic analyses

Alignment of the RNA-seq data to the *Drosophila melanogaster* reference genome (Release 6, Dm6) was performed using Subread package. RNA-seq data analysis was performed according to a module designed by COMBINE-Australia (Github: https://github.com/COMBINE-Australia/RNAseq-R) in RStudio and assisted by Perplexity (https://www.perplexity.ai/). FeatureCounts function in RSubread package was utilised to summarise reads into counts table in which features mapped to multiple genes were excluded. edgeR and limma packages were employed to analyse count data. To filter for lowly expressed genes, counts-per-million (CPM) were calculated and genes with CPM<2 (equivalent to count<10) were discarded. To remove composition biases between libraries, TMM normalisation was applied. To realise differential expression, counts data was transformed into logCPM using the voom function in the limma package. The empirical Bayes method was used to perform empirical Bayes shrinkage on the variances, estimate moderated t-statistics and generate p-values and logFC. To control for multiple testing during exploratory analysis of our RNA-seq data, the testing relative to a threshold (treat) function from the limma package was utilised to recalculate the moderated t-statistics and p-values for a FC cut-off of 1.5 and p-value of 0.05. RNA-seq results were plotted in RStudio using gplots, ggplot2, VennDiagram packages.

Gene Ontology (GO) enrichment analyses were performed on gene symbols extracted from org.Dm.eg.db package, using the topGO package in RStudio. Overrepresented GO terms were identified through Fisher's exact test with weight method on genes with p-value<0.05 after treat. To realise GO enrichment, differential expressed genes were compared with those of all known genes present in the annotation. The results were plotted in RStudio using the ggplot2 package.

Statistical analyses

At least three animals per genotype were used for all experiments. Statistical analyses and plotting were performed in GraphPad Prism 9. In graphs, data = mean ± standard error of the mean (SEM). n = lobes or clones as specified. For comparisons between two conditions, p-values were calculated by non-parametric Mann-Whitney tests when data show non-normally distribution. For comparisons between more than two conditions, p-values were calculated by Kruskal-Wallis tests for non-normally

distributed data. Dunn's tests were used to correct for multiple comparisons following Kruskal-Wallis tests. (*) $p<0.05$ (**) $p< 0.01$, (***) $p< 0.001$, (****) $p < 0.0001$, (ns) $p>0.05$.

Acknowledgements

We are grateful to Lei Zhang, Helena Richardson, Kieran Harvey, Tony Southall, Ward Odenwald, Alex Gould, Cedric Maurange, Tzumin Lee, Nicholas Sokol, Claude Desplan, Paul M Macdonald, and Kuniaki Saito for the generous sharing of antibodies and fly stocks. We thank Qian Dong and Tony Southall for critical reading of the manuscript; Abdul Jabbar Saiful Hilmi and Sofya Golenkina for assisting with the generation of *UAS-chinmo*^{RNAi} construct; Katrina Mitchell for assisting with RNA-seq data analyses. We thank the Bloomington *Drosophil*a Stock Centre (BDSC), Vienna *Drosophila* Resource Centre (VDRC), and Developmental Studies Hybridoma Bank (DSHB) for fly stocks and antibodies. We thank OZDros for *Drosophila* quarantine. We thank Centre for Advanced Histology and Microscopy (RRID:SCR_025432), Research Flow Core (RRID:SCR_025550), and Molecular Genomics Core (RRID:SCR_025695) at Peter MacCallum Cancer Centre for access and support. We thank Australian *Drosophila* Transgenic Facility for injection service. PKN is funded by a PhD scholarship from the Department of Anatomy and Physiology, The University of Melbourne and the Vingroup Science and Technology Scholarship Program for Overseas Study for Master's and Doctoral Degrees. LYC's laboratory is supported by funding from the NHMRC Ideas Grant (APP2011289).

Author contributions

PKN: Conceptualization; Formal analysis; Investigation; Methodology; Validation; Writing-original draft; Writing-review and editing. **FF:** Conceptualization; Formal analysis; Investigation; Methodology. **LYC:** Conceptualization; Resources; Formal analysis; Supervision; Funding acquisition; Investigation; Methodology; Validation; Project administration; Writing-original draft; Writing-review and editing.

Disclosure and competing interests statement

The authors declare no competing interests.

References

Arain, U., Islam, I. M., Valentino, P., & Erclik, T. (2022). *Concurrent temporal patterning of neural stem cells in the fly visual system* (p. 2022.10.13.512100). bioRxiv. https://doi.org/10.1101/2022.10.13.512100

Aughey, G. N., Forsberg, E., Grimes, K., Zhang, S., & Southall, T. D. (2023). NuRD-independent Mi-2 activity represses ectopic gene expression during neuronal maturation. *EMBO Reports*, *24*(4), e55362. https://doi.org/10.15252/embr.202255362

Bressan, R. B., Southgate, B., Ferguson, K. M., Blin, C., Grant, V., Alfazema, N., Wills, J. C., Marques-Torrejon, M. A., Morrison, G. M., Ashmore, J., Robertson, F., Williams, C. A. C., Bradley, L., Kriegsheim, A. von, Anderson, R. A., Tomlinson, S. R., & Pollard, S. M. (2021). Regional identity of human neural stem cells determines oncogenic responses to histone H3.3 mutants. *Cell Stem Cell*, *28*(5), 877-893.e9. https://doi.org/10.1016/j.stem.2021.01.016

Bruschi, M., Grill, J., & Guerrini-Rousseau, L. (2021). Pediatric brain tumors as a developmental disease. *Current Opinion in Oncology*, *33*(6), Article 6. https://doi.org/10.1097/CCO.0000000000000782

Chafino, S., Giannios, P., Casanova, J., Martín, D., & Franch-Marro, X. (2023). Antagonistic role of the BTB-zinc finger transcription factors Chinmo and Broad-Complex in the juvenile/pupal transition and in growth control. *eLife*, *12*, e84648. https://doi.org/10.7554/eLife.84648

Chen, X., Yang, W., Roberts, C. W. M., & Zhang, J. (2024). Developmental origins shape the paediatric cancer genome. *Nature Reviews Cancer*, *24*(6), 382–398. https://doi.org/10.1038/s41568-024-00684-9

Dillard, C., Narbonne-Reveau, K., Foppolo, S., Lanet, E., & Maurange, C. (2018). Two distinct mechanisms silence chinmo in Drosophila neuroblasts and neuroepithelial cells to limit their self-renewal. *Development*, *145*(2), Article 2. https://doi.org/10.1242/dev.154534

Dinges, N., Morin, V., Kreim, N., Southall, T. D., & Roignant, J.-Y. (2017). Comprehensive Characterization of the Complex *lola* Locus Reveals a Novel Role in the Octopaminergic Pathway via Tyramine Beta-Hydroxylase Regulation. *Cell Reports*, *21*(10), 2911–2925. https://doi.org/10.1016/j.celrep.2017.11.015

Egger, B., Boone, J. Q., Stevens, N. R., Brand, A. H., & Doe, C. Q. (2007). Regulation of spindle orientation and neural stem cell fate in the Drosophila optic lobe. *Neural Development*, *2*, 1. https://doi.org/10.1186/1749-8104-2-1

Farnsworth, D. R., Bayraktar, O. A., & Doe, C. Q. (2015). Aging Neural Progenitors Lose Competence to Respond to Mitogenic Notch Signaling. *Current Biology*, *25*(23), Article 23. https://doi.org/10.1016/j.cub.2015.10.027

Friedmann-Morvinski, D., & Verma, I. M. (2014). Dedifferentiation and reprogramming: Origins of cancer stem cells. *EMBO Reports*, *15*(3), 244–253. https://doi.org/10.1002/embr.201338254

Froldi, F., Szuperak, M., Weng, C.-F., Shi, W., Papenfuss, A. T., & Cheng, L. Y. (2015). The transcription factor Nerfin-1 prevents reversion of neurons into neural stem cells. *Genes & Development*, *29*(2), Article 2. https://doi.org/10.1101/gad.250282.114

Genovese, S., Clément, R., Gaultier, C., Besse, F., Narbonne-Reveau, K., Daian, F., Foppolo, S., Luis, N. M., & Maurange, C. (2019). Coopted temporal patterning governs cellular hierarchy, heterogeneity and metabolism in Drosophila neuroblast tumors. *eLife*, *8*, e50375. https://doi.org/10.7554/eLife.50375

Gibson, P., Tong, Y., Robinson, G., Thompson, M. C., Currle, D. S., Eden, C., Kranenburg, T. A., Hogg, T., Poppleton, H., Martin, J., Finkelstein, D., Pounds, S., Weiss, A., Patay, Z., Scoggins, M., Ogg, R., Pei, Y., Yang, Z.-J., Brun, S., … Gilbertson, R. J. (2010). Subtypes of medulloblastoma have distinct developmental origins. *Nature*, *468*(7327), 1095–1099. https://doi.org/10.1038/nature09587

Goeke, S., Greene, E. A., Grant, P. K., Gates, M. A., Crowner, D., Aigaki, T., & Giniger, E. (2003). Alternative splicing of lola generates 19 transcription factors controlling axon guidance in Drosophila. *Nature Neuroscience*, *6*(9), 917–924. https://doi.org/10.1038/nn1105

Harzer, H., Berger, C., Conder, R., Schmauss, G., & Knoblich, J. A. (2013). FACS purification of Drosophila larval neuroblasts for next-generation sequencing. *Nature Protocols*, *8*(6), 1088–1099. https://doi.org/10.1038/nprot.2013.062

Hassan, A., Araguas Rodriguez, P., Heidmann, S. K., Walmsley, E. L., Aughey, G. N., & Southall, T. D. (2020). Condensin I subunit Cap-G is essential for proper gene expression during the maturation of post-mitotic neurons. *eLife*, *9*, e55159. https://doi.org/10.7554/eLife.55159

Hofbauer, A., & Campos-Ortega, J. A. (1990). Proliferation pattern and early differentiation of the optic lobes in Drosophila melanogaster. *Roux's Archives of Developmental Biology*, *198*(5), Article 5. https://doi.org/10.1007/bf00377393

Ito, K., & Hotta, Y. (1992). Proliferation pattern of postembryonic neuroblasts in the brain of Drosophila melanogaster. *Developmental Biology*, *149*(1), Article 1. https://doi.org/10.1016/0012-1606(92)90270-Q

Jiang, Y., Seimiya, M., Schlumpf, T. B., & Paro, R. (2018). An intrinsic tumour eviction mechanism in Drosophila mediated by steroid hormone signalling. *Nature Communications*, *9*(1), Article 1. https://doi.org/10.1038/s41467-018-05794-1

Lanet, E., Gould, A. P., & Maurange, C. (2013). Protection of neuronal diversity at the expense of neuronal numbers during nutrient restriction in the Drosophila visual system. *Cell Reports*, *3*(3), Article 3. https://doi.org/10.1016/j.celrep.2013.02.006

Lee, T., & Luo, L. (1999). Mosaic Analysis with a Repressible Cell Marker for Studies of Gene Function in Neuronal Morphogenesis. *Neuron*, *22*(3), 451–461. https://doi.org/10.1016/S0896-6273(00)80701-1

Li, X., Erclik, T., Bertet, C., Chen, Z., Voutev, R., Venkatesh, S., Morante, J., Celik, A., & Desplan, C. (2013). Temporal patterning of Drosophila medulla neuroblasts controls neural fates. *Nature*, *498*(7455), Article 7455. https://doi.org/10.1038/nature12319

Liu, Z., Yang, C.-P., Sugino, K., Fu, C.-C., Liu, L.-Y., Yao, X., Lee, L. P., & Lee, T. (2015). Opposing intrinsic temporal gradients guide neural stem cell production of varied neuronal fates. *Science*, *350*(6258), 317–320. https://doi.org/10.1126/science.aad1886

Mackay, A., Burford, A., Carvalho, D., Izquierdo, E., Fazal-Salom, J., Taylor, K. R., Bjerke, L., Clarke, M., Vinci, M., Nandhabalan, M., Temelso, S., Popov, S., Molinari, V., Raman, P., Waanders, A. J., Han, H. J., Gupta, S., Marshall, L., Zacharoulis, S., … Jones, C. (2017). Integrated Molecular Meta-Analysis of 1,000 Pediatric High-Grade and Diffuse Intrinsic Pontine Glioma. *Cancer Cell*, *32*(4), 520-537.e5. https://doi.org/10.1016/j.ccell.2017.08.017

Marshall, G. M., Carter, D. R., Cheung, B. B., Liu, T., Mateos, M. K., Meyerowitz, J. G., & Weiss, W. A. (2014). The prenatal origins of cancer. *Nature Reviews Cancer*, *14*(4), 277–289. https://doi.org/10.1038/nrc3679

Maurange, C., Cheng, L., & Gould, A. P. (2008). Temporal transcription factors and their targets schedule the end of neural proliferation in Drosophila. *Cell*, *133*(5), Article 5. https://doi.org/10.1016/j.cell.2008.03.034

Morante, J., Erclik, T., & Desplan, C. (2011). Cell migration in Drosophila optic lobe neurons is controlled by eyeless/Pax6. *Development (Cambridge, England)*, *138*(4), Article 4. https://doi.org/10.1242/dev.056069

Narbonne-Reveau, K., Lanet, E., Dillard, C., Foppolo, S., Chen, C.-H., Parrinello, H., Rialle, S., Sokol, N. S., & Maurange, C. (2016). Neural stem cell-encoded temporal patterning delineates an early window of malignant susceptibility in Drosophila. *eLife*, *5*, e13463. https://doi.org/10.7554/eLife.13463

Narbonne-Reveau, K., & Maurange, C. (2019). Developmental regulation of regenerative potential in Drosophila by ecdysone through a bistable loop of ZBTB transcription factors. *PLOS Biology*, *17*(2), e3000149. https://doi.org/10.1371/journal.pbio.3000149

Nguyen, P.-K., & Cheng, L. Y. (2024). Drosophila medulla neuroblast termination via apoptosis, differentiation, and gliogenic switch is scheduled by the depletion of the neuroepithelial stem cell pool. *eLife*, *13*, e96876. https://doi.org/10.7554/eLife.96876

Pavinato, L., & Baggiolini, A. (2025). Oncogenic competence: Balancing mutations, cellular state, and microenvironment. *Trends in Cancer*. https://doi.org/10.1016/j.trecan.2025.01.002

Ren, Q., Yang, C.-P., Liu, Z., Sugino, K., Mok, K., He, Y., Ito, M., Nern, A., Otsuna, H., & Lee, T. (2017). Stem Cell-Intrinsic, Seven-up-Triggered Temporal Factor Gradients Diversify Intermediate Neural Progenitors. *Current Biology*, *27*(9), Article 9. https://doi.org/10.1016/j.cub.2017.03.047

Sieber, M. H., & Spradling, A. C. (2015). Steroid Signaling Establishes a Female Metabolic State and Regulates SREBP to Control Oocyte Lipid Accumulation. *Current Biology*, *25*(8), 993–1004. https://doi.org/10.1016/j.cub.2015.02.019

Southall, T. D., Davidson, C. M., Miller, C., Carr, A., & Brand, A. H. (2014). Dedifferentiation of Neurons Precedes Tumor Formation in lola Mutants. *Developmental Cell*, *28*(6), Article 6. https://doi.org/10.1016/j.devcel.2014.01.030

Sturm, D., Witt, H., Hovestadt, V., Khuong-Quang, D.-A., Jones, D. T. W., Konermann, C., Pfaff, E., Tönjes, M., Sill, M., Bender, S., Kool, M., Zapatka, M., Becker, N., Zucknick, M., Hielscher, T., Liu, X.-Y., Fontebasso, A. M., Ryzhova, M., Albrecht, S., … Pfister, S. M. (2012). Hotspot Mutations in H3F3A and IDH1 Define Distinct Epigenetic and Biological Subgroups of Glioblastoma. *Cancer Cell*, *22*(4), 425–437. https://doi.org/10.1016/j.ccr.2012.08.024

Syed, M. H., Mark, B., & Doe, C. Q. (2017). Steroid hormone induction of temporal gene expression in Drosophila brain neuroblasts generates neuronal and glial diversity. *eLife*, *6*, e26287. https://doi.org/10.7554/eLife.26287

Thummel, C. S. (2001). Molecular Mechanisms of Developmental Timing in *C. elegans* and *Drosophila*. *Developmental Cell*, *1*(4), 453–465. https://doi.org/10.1016/S1534-5807(01)00060-0

Truman, J. W., & Bate, M. (1988). Spatial and temporal patterns of neurogenesis in the central nervous system of Drosophila melanogaster. *Developmental Biology*, *125*(1), Article 1. https://doi.org/10.1016/0012-1606(88)90067-X

Vissers, J. H. A., Froldi, F., Schröder, J., Papenfuss, A. T., Cheng, L. Y., & Harvey, K. F. (2018). The Scalloped and Nerfin-1 Transcription Factors Cooperate to Maintain Neuronal Cell Fate. *Cell Reports*, *25*(6), Article 6. https://doi.org/10.1016/j.celrep.2018.10.038

Wu, Y.-C., Chawla, G., & Sokol, N. (2020). Let-7-Complex MicroRNAs Regulate Broad-Z3, Which Together with Chinmo Maintains Adult Lineage Neurons in an Immature State. *G3 Genes|Genomes|Genetics*, *10*(4), 1393–1401. https://doi.org/10.1534/g3.120.401042

Xu, J., Hao, X., Yin, M.-X., Lu, Y., Jin, Y., Xu, J., Ge, L., Wu, W., Ho, M., Yang, Y., Zhao, Y., & Zhang, L. (2017). Prevention of medulla neuron dedifferentiation by Nerfin-1 requires inhibition of Notch activity. *Development (Cambridge, England)*, *144*(8), Article 8. https://doi.org/10.1242/dev.141341

Yang, C.-P., Samuels, T. J., Huang, Y., Yang, L., Ish-Horowicz, D., Davis, I., & Lee, T. (2017). Imp and Syp RNA-binding proteins govern decommissioning of Drosophila neural stem cells. *Development*, *144*(19), Article 19. https://doi.org/10.1242/dev.149500

Yasugi, T., Umetsu, D., Murakami, S., Sato, M., & Tabata, T. (2008). Drosophila optic lobe neuroblasts triggered by a wave of proneural gene expression that is negatively regulated by JAK/STAT. *Development*, *135*(8), 1471–1480. https://doi.org/10.1242/dev.019117

Zhou, Y., Yang, Y., Huang, Y., Wang, H., Wang, S., & Luo, H. (2019). Broad Promotes Neuroepithelial Stem Cell Differentiation in the Drosophila Optic Lobe. *Genetics*, *213*(3), Article 3. https://doi.org/10.1534/genetics.119.302421

Zhu, H., Zhao, S. D., Ray, A., Zhang, Y., & Li, X. (2022). A comprehensive temporal patterning gene network in Drosophila medulla neuroblasts revealed by single-cell RNA sequencing. *Nature Communications*, *13*(1), 1247. https://doi.org/10.1038/s41467-022-28915-3

Zhu, S., Lin, S., Kao, C.-F., Awasaki, T., Chiang, A.-S., & Lee, T. (2006). Gradients of the Drosophila Chinmo BTB-Zinc Finger Protein Govern Neuronal Temporal Identity. *Cell*, *127*(2), 409–422. https://doi.org/10.1016/j.cell.2006.08.045

Figure 1: *nerfin-1^{159}* dedifferentiated NBs are selectively eliminated in the OL during pupal development

(A-A') Schematic depicting **(A)** the frontal view and **(A')** the side view of the larval CNS that consists of the central brain (CB), the ventral nerve cord (VNC) and the optic lobes (OLs). Representative confocal images of the larval brain are taken from either Superficial or Deep layers.

(B) Schematic summarising our experimental procedure. MARCM or flip-out clones are induced at 24h after larval hatching (ALH). Larval brains are dissected at wandering L3 stage and pupal brains are dissected at 48h after pupal formation (APF) if not specified.

(C-D) Representative single confocal sections in the deep layers of **(C-C')** the brain lobe (including the CB and OL), and **(D-D')** the VNC with *nerfin-1^{159}* clones (yellow dash lines) at wandering L3 stage. In all regions, *nerfin-1^{159}* clones exhibit ectopic NBs marked by Dpn (magenta). GFP (green), DAPI (blue). White dash lines indicate the CB/OL borders.

(E-F) Representative maximum projections of **(E-E')** the brain lobe and **(F-F')** the VNC at 48h APF. In the OL, *nerfin-1^{159}* cells are dispersed and do not express Dpn (arrowheads). In the CB and VNC, *nerfin-1^{159}* clones (yellow dash lines) form tumours enriched with ectopic Dpn^{+} NBs. DAPI (blue), GFP (green), Dpn (magenta).

(G-H) Representative maximum projections of **(G-G')** the CB/OL and **(H-H')** the VNC at 48h APF with *nerfin-1^{159}* clones. In the OL (white dash lines), *nerfin-1^{159}* cells express neither the mature NB marker Mira nor the mitotic marker PH3 (arrowheads). In the CB and VNC, *nerfin-1^{159}* clones (yellow dash lines) form tumours enriched with ectopic Mira^{+}PH3^{+} NBs. DAPI (blue), GFP (green), Mira (magenta), PH3 (grey).

Figure 2: *nerfin-1^{159}* dedifferentiated NBs are eliminated Pros-mediated terminal differentiation in the pupal OL

(A-B) Representative single confocal sections of **(A-A''')** the OL and **(B-B''')** the VNC with *nerfin-1^{159}* clones at 48h APF. **(A'-A''')** and **(B'-B''')** are insets indicated by boxes in **(A)** and **(B)**, respectively. GFP (green), Elav (red), Repo (grey). In the VNC, yellow dash lines outline the mutant clone. Yellow arrowhead indicates Elav^{-}Repo^{-} mutant cell. Cyan and magenta arrowheads indicate Elav^{+}Repo^{-} and Elav^{-}Repo^{+} mutant cells, respectively.

(C) Quantifications of the neuron ratio in *nerfin-1^{159}* clones in the OL and the VNC at 48h APF. Mann-Whitney test: *p=0.032. VNC: n=4, m=0.17 ± 0.016. OL: n=5, m=0.28 ± 0.028.

(D-E) Representative single confocal sections in the deep layers of the brain lobes with **(D-D')** *pros^{RNAi}* and **(E-E')** *pros^{RNAi};nerfin-1^{159}* clones (yellow dash lines) at wandering L3 stage. GFP (green), Dpn (magenta). White dash lines outline the CB/OL borders.

(F-I) Representative maximum projections of the OL (dash lines) at 48h APF with **(F-F')** *nerfin-1^{159}*, **(G-G')** *pros^{RNAi}*, **(H-H')** *pros^{RNAi};nerfin-1^{159}* and **(I-I')** *gcm^{RNAi};nerfin-1^{159}* clones. Arrowheads indicate ectopic NBs. DAPI (blue), GFP (green), Dpn (magenta).

(J) Quantifications of the NB ratio of *nerfin-1^{159}*, *pros^{RNAi}*, and *pros^{RNAi};nerfin-1^{159}* clones in the OLs at 48h APF. Kruskal-Wallis test: (ns)p=0.220, **p=0.002. *nerfin-1^{159}*: n=6, m=0.001 ± 0.001. *pros^{RNAi}:* n=7, m= 0.094 ± 0.017. *pros^{RNAi};nerfin-1^{159}*: n=6, m=0.21 ± 0.039.

(K) Quantifications of the NB ratio of *nerfin-1^{159}* and *gcm^{RNAi};nerfin-1^{159}* clones in the OLs at 48h APF. Mann-Whitney test: (ns) p=0.470. *nerfin-1^{159}*: n=6, m=0.007 ± 0.005. *gcm^{RNAi};nerfin-1^{159}*: n=7, m=0.008 ± 0.004.

Figure 3: Chinmo promotes the persistence of *nerfin-1^{159}* ectopic NBs in the pupal CNS

(A-C) Representative single confocal sections of *nerfin-1^{159}* clones (dash lines) in **(A-A'')** the CB, **(B-B'')** the VNC and **(C-C'')** the OL at wandering L3 stage. DAPI (blue), GFP (green), Dpn (magenta), Chinmo (grey).

(D-E) Representative single confocal sections of **(D-D'')** *nerfin-1^{159}* and **(E-E'')** *chinmo^{RNAi};nerfin-1^{159}* clones (dash lines) in the VNC at wandering L3 stage. DAPI (blue), GFP (green), Dpn (magenta), Chinmo (grey).

(F-G) Representative maximum projections of the VNC with **(F-F')** *nerfin-1^{159}* and **(G-G')** *chinmo^{RNAi};nerfin-1^{159}* clones (dash lines) at 48h APF. DAPI (blue), GFP (green), Dpn (magenta).

(H) Quantifications of the NB ratio of *nerfin-1^{159}* and *chinmo^{RNAi};nerfin-1^{159}* clones in the VNC at 48h APF. Mann-Whitney test: **p=0.001. *nerfin-1^{159}*: n=6, m=0.16 ± 0.055. *chinmo^{RNAi};nerfin-1^{159}*: n=7, m=0.015 ± 0.004.

(I-J) Representative maximum projections of the OLs (dash lines) at 24h APF with **(I-I')** *nerfin-1^{RNAi};mCherry^{RNAi}* and **(J-J')** *nerfin-1^{RNAi};UAS-chinmo^{FL}* flip-out clones. The expression of *UAS-chinmo^{FL}* results in persistent ectopic NBs (arrowheads). DAPI (blue), GFP (green), Dpn (magenta).

822 **(K)** Quantifications of the NB ratio of *nerfin-1^{RNAi};mCherry^{RNAi}* and *nerfin-1^{RNAi};UAS-chinmo^{FL}* flip-out clones in the
823 OLs at 24h APF. Mann-Whitney test: **p=0.004. *nerfin-1^{RNAi};mCherry^{RNAi}*: n=5, m=0.00 ± 0.00. *nerfin-1^{RNAi};UAS-*
824 *chinmo^{FL}*: n=6, m=0.175 ± 0.011.

825 **(L-N)** Representative single confocal sections of the OLs (dash lines) at 48h APF with **(L-L'')** *UAS-EcR^{DN}*, **(M-M'')**
826 *nerfin-1^{159}* and **(N-N'')** *UAS-EcR^{DN};nerfin-1^{159}* clones. Persistent ectopic NBs (arrowheads) are present in *UAS-*
827 *EcR^{DN};nerfin-1^{159}* clones. This is accompanied by the upregulation of Chinmo (blue). GFP (green), Dpn (magenta).

828 **(O)** Quantifications of NB ratio of *UAS-EcR^{DN}, nerfin-1^{159}*, and *UAS-EcR^{DN};nerfin-1^{159}* clones in the OLs at 48h
829 APF. Kruskal-Wallis test and Dunn's test to correct for multiple comparison: ****p<0.0001, **p=0.002. *UAS-EcR^{DN}*:
830 n=8, m=0.00 ± 0.00. *nerfin-1^{159}*: n=8, m=0.002 ± 0.001. *UAS-EcR^{DN};nerfin-1^{159}*: n=8, m=0.017 ± 0.003.

831

832 **Figure 4: Lola promotes temporal progression in the larval medulla NE**

833 **(A-A')** Representative single confocal sections in the deep layers of the OL at wandering L3 stage with *lola^{E76}*
834 clones (dash lines). DAPI (blue), GFP (green), Dpn (magenta).

835 **(B-B')** Representative maximum projections of the OLs (dash lines) at 48h APF with *lola^{E76}* clones (arrowheads).
836 GFP (green), Dpn (magenta), Chinmo (grey).

837 **(C-C')** Representative maximum projections of the OLs (dash lines) at 48h APF with *lola^{E76}* clones (arrowheads).
838 GFP (green), PH3 (grey).

839 **(D)** Schematic depicting the organisation of the larval OL medulla. On the superficial layers, symmetrically dividing
840 NE cells continuously convert into NBs upon a proneural wave. NBs undergo asymmetric cell division to self-renew
841 and to produce medulla neurons (and glia) into the deep layers.

842 **(E-H)** Representative single confocal sections of the brain lobes expressing **(E-F)** Lola.I::GFP and **(G-H)** Nerfin-
843 1::GFP at wandering L3 stage. **(F-F''')** and **(H-H''')** are insets of the boxed areas in **(E)** and **(G)**, respectively. DAPI
844 (blue), PatJ marks the apical membrane of NE (grey), Dpn marks the NBs (magenta), GFP (green). Dash lines
845 outline the NE. Arrowheads indicate NBs.

846 **(I)** mRNA expression represented as normalised counts of the NE temporal factors *Imp, chinmo, mamo, Syp, br,*
847 *Eip93F* from RNA-sequencing data of wildtype (WT) and *lola^{E76}* cells from the late larval OLs. Descriptive statistics
848 are detailed in Table 1.

849 **(J)** Schematic depicting temporal series in the NE adapted from Arain et al., (2022). The early temporal window is
850 characterised by the expression of Imp and Chinmo. The late temporal window is characterised by the expression
851 of Br, Syp, and Eip93F.

852 **(K-L)** Representative single confocal section on the superficial layers of the brain lobes containing *lola^{E76}* clones
853 (yellow dash lines) at wandering L3 stage. GFP (green), DE-Cad (red) marks the NE architecture. **(K-K''')** In *lola^{E76}*
854 NE cells, Imp (grey) is upregulated whereas Mamo (blue) is downregulated compared to wildtype surrounding cells.
855 **(L-L''')** In *lola^{E76}* NE cells, Syp (grey) is downregulated whereas Chinmo (blue) is upregulated compared to wildtype
856 cells. White dash lines indicate the CB/OL borders.

857 **(M)** Summary schematic of the phenotype of *lola* loss-of-function in the larval NE compared to wildtype and *nerfin-*
858 *1* loss-of-function.

859

860 **Figure 5: Chinmo and Imp promote the persistence of *lola^{E76}* ectopic NBs in the pupal OL**

861 **(A-B)** Representative single confocal sections of **(A-A'')** *lola^{E76}* and **(B-B'')** *lola^{E76};chinmo^{RNAi}* clones (dash lines)
862 in the deep layers of the OLs at wandering L3 stage. GFP (green), Dpn (magenta), Chinmo (grey).

863 **(C-E)** Representative maximum projections of the OLs (dash lines) at 48h APF with **(C-C')** *lola^{E76}*, **(D-D')**
864 *lola^{E76};chinmo^{RNAi}* and **(E-E')** *lola^{E76};Imp^{RNAi}* clones. Arrowheads indicate ectopic NBs. DAPI (blue), GFP (green),
865 Dpn (magenta).

866 **(F)** Quantifications of the NB ratio of *lola^{E76}*, *lola^{E76};chinmo^{RNAi},* and *lola^{E76};Imp^{RNAi}* clones in the OLs at 48h APF.
867 Kruskal-Wallis test and Dunn's test to correct for multiple comparison: *p=0.048, **p=0.002. *lola^{E76}*: n=7, m=0.096
868 ± 0.019. *lola^{E76};chinmo^{RNAi}*: n=9, m=0.030 ± 0.004, *lola^{E76};Imp^{RNAi}*: n=6, m=0.021 ± 0.015.

869 **(G-G'')** Representative single confocal section of the OL (dash lines) at 48h APF with *lola^{E76}* clones (arrowheads).
870 G'-G'' are magnified insets of box indicated in G. GFP (green), EcR (red).

871 **(H)** Clonal induction scheme. In general, clones are induced at 24h ALH during the early temporal window. In Figure
872 4I-J, clones are induced at 60h ALH, bypassing the early Chinmo^{+} time window.

(I-I'''') Representative single confocal section in the deep layers of the brain lobe with *lola*^{E76} clones (yellow dash lines) at wandering L3 stage, in which mutant clones are induced at 60h ALH. RFP (red), Dpn (cyan), Syp (grey), Chinmo (blue). White dash lines indicate the CB/OL border.

(J-J'''') Representative maximum projection of the OL (dash lines) at 48h APF with *lola*^{E76} clones (arrowheads), in which mutant clones are induced at 60h ALH. RFP (red), Dpn (cyan), Syp (grey), Chinmo (blue).

Figure 6: Temporal progression is delayed in *lola*^{E76} dedifferentiated NBs

(A) Schematic depicting the temporal series in the medulla NBs.

(B) Schematic depicting the side view of the larval CNS. Representative confocal images of the larval brain are taken from either Superficial (for Figure 5C-F) or Deep (for Figure 5G-H) layers.

(C-F) Representative single confocal sections of **(C-C'', D-D'')** WT control and (**E-E'', F-F''**) *lola*^{E76} clones on the superficial layers of the medulla at wandering L3 stage. **(C-C'', E-E'')** GFP (green), Dpn (magenta), Ey (grey). **(D-D'', F-F'')** GFP (green), Dpn (magenta), Slp (cyan), Tll (grey). Dash lines outline mutant clones.

(G-H) Representative single confocal sections of *lola*^{E76} clones (dash lines) in the deep layers of the medulla. **(G-G'')** GFP (green), Dpn (magenta), Ey (grey). Arrowheads indicate NBs expressing Ey. **(H-H'')** GFP (green), Dpn (magenta), Slp (cyan), Tll (grey). Arrowheads indicate NBs expressing Slp.

(I-J) Representative single confocal section of *lola*^{E76} clones (dash lines) in the OL at 48h APF. **(I-I'')** GFP (green), Dpn (magenta), Ey (grey). Arrowheads indicate NBs expressing Ey. **(J-J'')** GFP (green), Dpn (magenta), Slp (cyan), Tll (grey). Arrowheads indicate NBs expressing Tll.

(K) Quantifications of the NB ratio expressing Ey, Slp, and Tll in *lola*^{E76} clones at wandering L3 stage and 48h APF in the OLs. Descriptive statistics are detailed in Table 3.

(L) Summary schematic depicting the delayed temporal progression in *lola*^{E76} dedifferentiated NBs (dNBs) compared to WT NBs. Early temporal identity is represented in yellow, mid-temporal identity in cyan and late temporal identity in grey.

Figure 7: Lola expression in *nerfin-1* loss-of-function clones promotes elimination of ectopic NBs in the pupal OL

(A) Representative single confocal section in the deep layers of the brain lobe at wandering L3 stage with *nerfin-1*^{RNAi} flip-out clones (yellow dash lines). *nerfin-1*^{RNAi} clones display ectopic NBs that express Lola.I::GFP (green). RFP (red), Mira (magenta). White dash lines indicate the CB/OL borders.

(B) *lola* normalised counts from RNA-seq data of WT and *nerfin-1*^{159} cells collected from the late larval OLs. Descriptive statistics are detailed in Table 4.

(C-D) Representative single confocal sections in the deep layers of the brain lobes at wandering L3 stage with **(C-C')** *lola*^{RNAi} and **(D-D')** *lola*^{RNAi};*nerfin-1*^{159} clones (yellow dash lines). Ectopic NBs in the deep section of the medulla indicate neuronal dedifferentiation. DAPI (blue), GFP (green), Dpn (magenta). White dash lines indicate the CB/OL borders.

(E-F) Representative maximum projections of the OLs (dash lines) at 48h APF with **(E-E')** *lola*^{RNAi} and **(F-F')** *lola*^{RNAi};*nerfin-1*^{159} clones. DAPI (blue), GFP (green), Dpn (magenta). Arrowheads indicate ectopic NBs in the OLs.

(G) Quantifications of the NB ratio of *nerfin-1*^{159}, *lola*^{RNAi} and *lola*^{RNAi};*nerfin-1*^{159} clones in the OLs at 48h APF. Kruskal-Wallis test and Dunn's test to correct for multiple comparisons: ****$p<0.0001$, *$p=0.024$. *nerfin-1*^{159}: n=13, m=0.005 ± 0.002. *lola*^{RNAi}: n=9, m=0.014 ± 0.005. *lola*^{RNAi};*nerfin-1*^{159}: n=12, m=0.038 ± 0.006.

(H) Summary schematic: In the CB/VNC, Chinmo expression inherited from dedifferentiating *nerfin-1* loss-of-function (LOF) neurons promotes persistence of dedifferentiated NBs (dNBs) in the pupal stages. In contrast, in the OL, ecdysone signalling represses Chinmo expression in *nerfin*-1 LOF clones, resulting in the elimination of dNBs through terminal differentiation and apoptosis. Lola LOF in the OL medulla ectopically upregulates Chinmo in the NE and dedifferentiating neurons to promote dNB persistence in the pupal OL.